Bioorganic Chemistry 167 (2025) 109243

Contents lists available at ScienceDirect

Bioorganic Chemistry

journal homepage: www.elsevier.com/locate/bioorg

Synthesis, carbonic anhydrase inhibition and *in silico* insights of 4-formyl-2-nitrophenyl naphthalene-2-sulfonate hybrid thiosemicarbazones

Khawar Abbas [a,1], Muhammad Islam [b,c,1], Muhammad Tayyab [a], Mariya al-Rashida [d], Parham Taslimi [e], Talha Islam [d], Nastaran Sadeghian [e], Halil Şenol [f], Abdullah K. Alanazi [g], Silvia Schenone [h,*], Zahid Shafiq [a,*]

[a] Institute of Chemical Sciences, Bahauddin Zakariya University, 60800 Multan, Pakistan
[b] Department of Basic Sciences and Humanities (Chemistry), Muhammad Nawaz Sharif University of Engineering and Technology (MNSUET), 60000 Multan, Pakistan
[c] School of Pharmaceutical Science and Technology, Tianjin University, 92 Weijin Road, Tianjin 300072, China
[d] Department of Chemistry, Forman Christian College (A Chartered University) Lahore, Pakistan
[e] Department of Biotechnology, Faculty of Science, Bartin University, 74110 Bartin, Türkiye
[f] Bezmialem Vakif University, Faculty of Pharmacy, Department of Pharmaceutical Chemistry, 34093, Fatih, Istanbul, Türkiye
[g] Department of Chemistry, College of Science, Taif University, Taif, Saudi Arabia
[h] Department of Pharmacy, University of Genoa, Viale Benedetto XV, 3, Genoa 16132, Italy

ARTICLE INFO

Keywords:
4-Formyl-2-nitrophenyl naphthalene-2-sulfonate
Carbonic anhydrase
Thiosemicarbazones
Molecular docking
In silico studies

ABSTRACT

A novel series of thiosemicarbazones derived from 4-formyl-2-nitrophenyl naphthalene-2-sulfonate is synthesized and assessed for inhibitory potential against human carbonic anhydrase isoforms hCA I and hCA II and metal chelating properties. Among the tested compounds, **6 l** exhibited the most potent inhibition with (IC_{50} = 88.43 ± 3.25 nM) (K_i = 73.70 ± 3.47 nM) for hCA I and (IC_{50} = 61.82 ± 0.60 nM) (K_i = 55.22 ± 5.32 nM) for hCA II. Remarkably, compound **6 l** exhibited greater potency than the reference drug acetazolamide (IC_{50} = 290.50 ± 9.12 nM for hCA I) and (IC_{50} = 177.03 ± 6.08 nM for hCA II). Additionally, the IC_{50} values of metal chelation for novel compounds ranged from (9.43 ± 0.80 to 75.24 ± 8.35 nM). SAR analysis indicated that dichlorophenyl substituent having electron withdrawing effect played a key role in enhancing inhibitory activity. To support these findings, molecular docking and dynamics simulations were performed to investigate the binding interactions and potential inhibitory mechanisms. The results highlight the significant inhibitory potential of the synthesized thiosemicarbazones as carbonic anhydrase inhibitors, suggesting their suitability for future development in treating conditions related to carbonic anhydrase disorders.

1. Introduction

Carbonic anhydrases are commonly occurring metalloenzymes in both eukaryotes and prokaryotes [1]. These enzymes catalyze the rapid conversion of CO_2 into HCO_3^-, a reaction essential for numerous physiological functions [2]. Carbonic anhydrases (CAs) play vital roles in various physiological processes, including pH regulation, CO_2 transport, and cerebrospinal fluid formation [3,4]. Dysregulation of specific CA isoforms, particularly hCA I and hCA II, has been implicated in various pathological conditions, including glaucoma, obesity, epilepsy, and cancer-related metabolic reprogramming [5–7]. The structural diversity of CAs is reflected in their classification into distinct families, each characterized by unique features and evolutionary origins [8]. Inhibiting CAs holds therapeutic potential for the treatment of several diseases, such as glaucoma, diabetes, epilepsy and Alzheimer's disease [6,9,10].

The carbonic anhydrase (CA) superfamily is classified into five distinct classes: α, β, γ, δ, and ζ [11]. Among these, hCA I and hCA II are important due to their roles in tissue repair, pH balance, and electrolyte secretion. hCA II, the most abundant isoform, is present in red blood cells, the gastrointestinal tract, lungs and kidneys and various cancers such as urothelial carcinoma and malignant brain tumors [12–14]. hCA I is primarily located in the gastrointestinal tract (GT) and erythrocytes [15].

Targeting specific CA isoforms is strongly associated with

* Corresponding authors.
E-mail addresses: silvia.Schenone@unige.it (S. Schenone), zahidshafiq@bzu.edu.pk (Z. Shafiq).
[1] Contributed equally

https://doi.org/10.1016/j.bioorg.2025.109243
Received 10 August 2025; Received in revised form 14 October 2025; Accepted 11 November 2025
Available online 15 November 2025

therapeutic applications. CA I is a cytosolic isoform predominantly expressed in erythrocytes, gastrointestinal tract, and eyes. Although it exhibits relatively low catalytic activity compared to other isoenzymes, it plays an important role in maintaining acid-base balance and has been implicated in pathological conditions such as retinal and cerebral edema. Owing to its abundance in erythrocytes, CA I is selected as a reference isoform in inhibition studies [16]. CA II inhibitors are widely used in medicine due to their diuretic, anti-glaucoma, and anti-epileptic properties [6,17,18] and are important in managing conditions such as epilepsy, edema, altitude sickness, and glaucoma [12,19]. CA II inhibitors, such as ethoxzolamide (EZA), [20] methazolamide (MZA), [21] and acetazolamide (AZA), [13] are effective but have limited selectivity. Inhibiting CA II and other isoenzymes may lead to adverse effects such as drowsiness, fatigue, and gastrointestinal disturbances [12,22–24].

Thiosemicarbazones (TSCs) are Schiff base ligands known for their structural flexibility and functional groups that enable strong binding to metals and DNA [25]. Their electron-donating moieties play a vital role in coordinating metal ions, contributing to their broad therapeutic potential [26]. Studies have demonstrated their biological and pharmacological properties, including antiviral [27], antimalarial [28], antitumor [29–34], anti-inflammatory, and cytotoxic effects [35,36].

Aryl sulfonate esters are highly valued in research because of their distinctive biological activities. In synthetic chemistry, they serve as important building blocks and key intermediates, synthesized by the reaction of phenolic compounds with sulfonyl chlorides [37]. These compounds have exhibited a variety of pharmacological properties, such as antioxidant, antiviral, anticholinesterase [38,39], anticancer, and carbonic anhydrase inhibitory activities [40–42].

The development of dual or multi-target pharmaceuticals has recently attracted considerable attention in medicinal chemistry [43–45]. Molecular hybridization has proven particularly effective for designing multi-target drug candidates aimed at treating complex diseases [46,47].

In the present study, we adopted this strategy to synthesize potential inhibitors targeting both forms. Specifically, a series of 4-formyl-2-nitrophenyl naphthalene-2-sulfonate-based thiosemicarbazones **6(a–t)** were prepared by reacting 4-formyl-2-nitrophenyl naphthalene-2-sulfonate with various thiosemicarbazide derivatives. Previously reported thiosemicarbazones and sulfonate ester-based hCA inhibitors are illustrated in Fig. 1 [48–53].

2. Results and discussion

2.1. Chemistry

A novel series of **6(a–t)** was synthesized by modifying the O—H group in 4-hydroxybenzaldehyde. Firstly, sonication of 4-hydroxybenzaldehyde **(1)** with nitric acid was done using DCM as a solvent to produce 4-hydroxy-3-nitrobenzaldehyde **(2)**. Secondly, 4-formyl-2-nitrophenyl naphthalene-2-sulfonate **(4)** was synthesized by reacting compound **(2)** with naphthalene-2-sulfonoyl chloride **(3)** at 0 °C using triethylamine and DMF for 1 h. Further, the corresponding thiosemicarbazones derivatives **6(a-t)** were synthesized by reacting 4-formyl-2-nitrophenyl naphthalene-2-sulfonate **(4)** and substituted thiosemicarbazides **5(a–t).** The synthetic pathway for the synthesis of 4-formyl-2-nitrophenyl naphthalene-2-sulfonate derived thiosemicarbazones **6(a-t)** is illustrated in Scheme 1.

2.2. Enzyme inhibition assay

The inhibition potential of novel compounds was evaluated against the hCA I and hCA II enzymes using acetazolamide as standard. As shown in Table 1, 4-formyl-2-nitrophenyl naphthalene-2-sulfonate-based TSCs **6(a-t)** showed significant inhibitory activity against hCA I and hCA II isoforms.

The newly derived compounds inhibited hCA I and hCA II efficiently at low nanomolar concentrations. For hCA I, IC_{50} values ranged from 88.43 ± 3.25 nM (K_i = 73.70 ± 3.47 nM) to 380.07 ± 8.32 nM (K_i = 362.27 ± 11.23 nM) and hCA II from 88.43 ± 3.25 nM (K_i = 73.70 ± 3.47) to 277.37 ± 3.91 (K_i = 270.38 ± 6.18 nM). In contrast, acetazolamide (AZA), used inhibitor with broad-spectrum activity against carbonic anhydrase isoforms, demonstrated comparatively lower potency (IC_{50} = 290.50 ± 9.12 nM) (K_i = 265.17 ± 14.66 nM) for hCA I and (IC_{50} = 177.03 ± 6.08 nM) (K_i = 151.41 ± 3.29 nM) for hCA II,

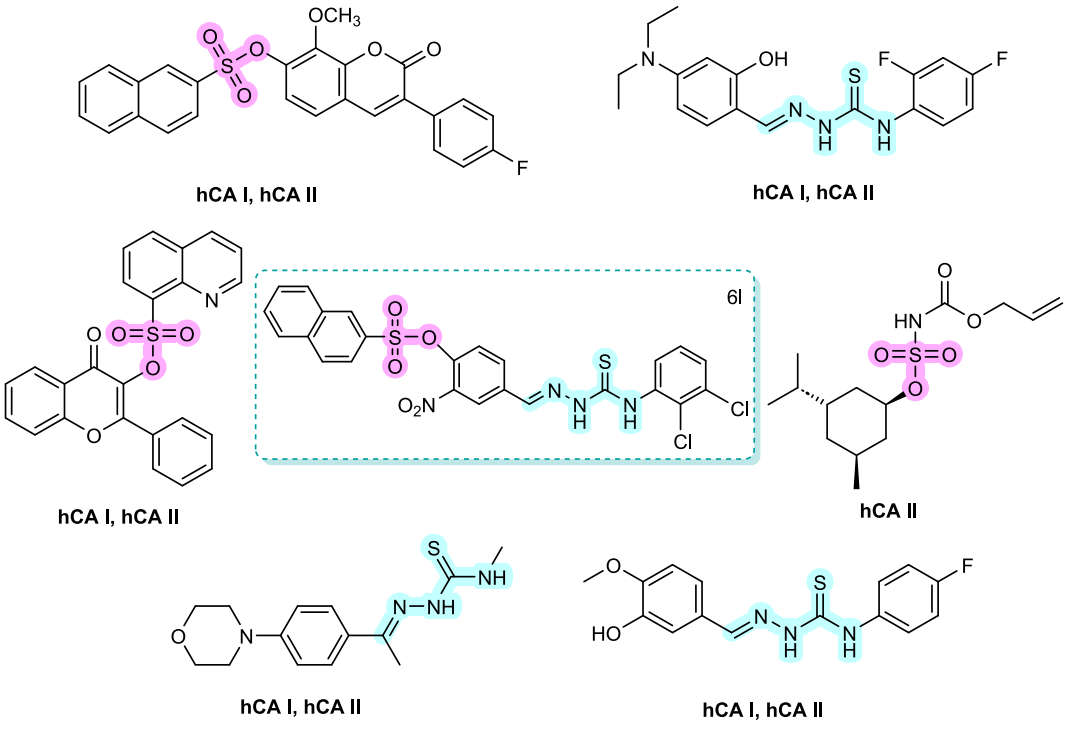

Fig. 1. Reported thiosemicarbazones and aryl sulphonates derived hCA I and hCA II inhibitors.

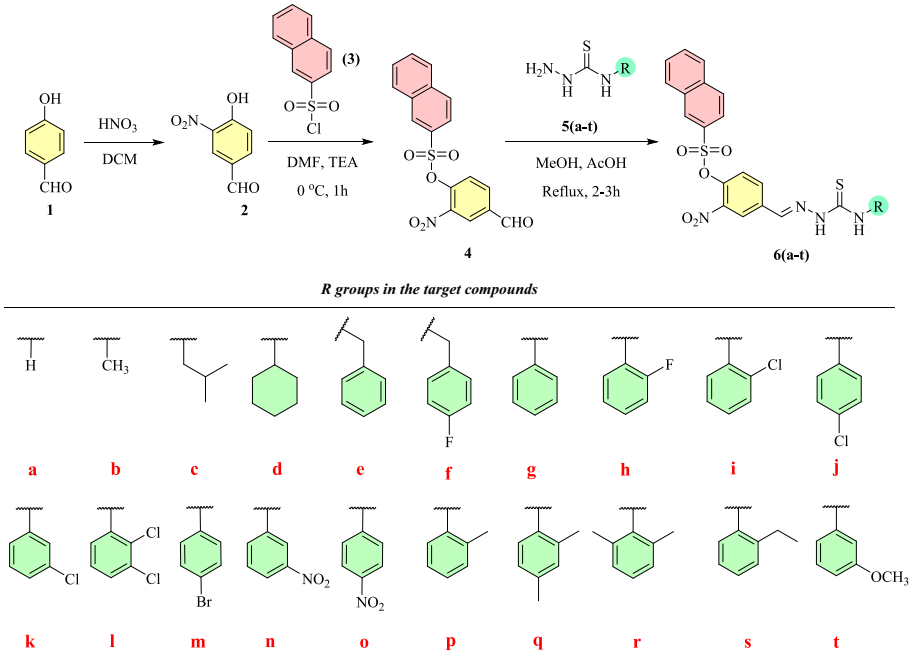

Scheme 1. Synthetic pathway of thiosemicarbazones derivatives **6(a-t)**

Table 1
IC_{50} and **K_i** values of novel compounds against **hCA I** and **hCA II.**

Codes	IC_{50} (nM)			K_i (nM)	
	Metal chelating	hCA I	hCA II	hCA I	hCA II
6a	42.06 ± 7.24	249.28 ± 6.12	166.52 ± 5.47	233.46 ± 8.64	149.86 ± 4.31
6b	47.23 ± 4.62	247.09 ± 9.31	128.46 ± 2.49	226.47 ± 8.22	117.41 ± 2.35
6c	75.24 ± 8.35	380. 07 ± 8.32	190.20 ± 5.38	362.27 ± 11.23	181.71 ± 7.06
6d	75.06 ± 5.36	212.05 ± 11.48	152.38 ± 1.43	206.53 ± 11.73	141.34 ± 3.42
6e	53.06 ± 4.02	286.47 ± 8.13	138.23 ± 2.38	221.53 ± 8.42	122.81 ± 5.12
6f	11.31 ± 0.57	113.52 ± 4.35	82.82 ± 3.24	95.62 ± 5.85	76.97 ± 3.66
6 g	51.22 ± 3.75	235.48 ± 7.23	133.35 ± 2.77	216.57 ± 11.56	129.33 ± 5.09
6 h	9.43 ± 0.80	108.60 ± 7.32	93.16 ± 2.06	100.15 ± 7.28	81.36 ± 4.05
6i	62.58 ± 5.70	174.51 ± 7.38	119.54 ± 1.02	163.41 ± 7.09	105.27 ± 4.77
6j	56.13 ± 3.21	167.30 ± 5.22	126.01 ± 1.22	158.11 ± 4.30	102.19 ± 4.42
6 k	37.09 ± 4.52	189.78 ± 6.44	126.23 ± 1.19	170.19 ± 6.91	104.01 ± 3.09
6 l	10.86 ± 0.16	88.43 ± 3.25	61.82 ± 0.60	73.70 ± 3.47	55.22 ± 5.32
6 m	14.95 ± 3.64	116.18 ± 6.23	88.15 ± 1.36	102.44 ± 4.76	73.33 ± 5.16
6n	11.14 ± 1.46	146.05 ± 5.41	123.40 ± 1.23	111.05 ± 5.30	100.27 ± 4.22
6o	13.85 ± 3.18	179.92 ± 6.68	115.62 ± 1.39	165.53 ± 7.47	106.52 ± 3.44
6p	40.37 ± 3.77	360.80 ± 6.05	275.25 ± 3.62	342.05 ± 8.87	252.43 ± 7.58
6q	67.04 ± 5.01	289.32 ± 7.59	147.35 ± 3.54	229.14 ± 6.33	134.27 ± 3.94
6r	59.34 ± 6.14	342.21 ± 9.19	170.24 ± 3.19	331.06 ± 13.21	153.59 ± 7.54
6 s	64.77 ± 5.04	368.29 ± 10.71	277.37 ± 3.91	320.23 ± 10.74	270.38 ± 6.18
6 t	45.03 ± 5.51	140.26 ± 5.91	116.73 ± 2.42	124.06 ± 5.05	107.42 ± 2.55
AZA*	–	290.50 ± 9.12	177.03 ± 6.08	265.17 ± 14.66	151.41 ± 3.29
EDTA**	13.28 ± 0.98	–	–	–	–

highlighting the greater inhibition potential of the novel compounds. Among all the synthesized derivatives, compound **6 l** exhibited the strongest inhibition potential towards both hCA I and hCA II.

2.3. Structure activity relationship

SAR analysis of novel compounds **6(a-t)** was primarily influenced by the nature of the R group attached to the thiosemicarbazone moiety. Their inhibitory activity was examined against the hCA I and hCA II isoforms. Acetazolamide (AZA) was used as reference compound, exhibiting IC_{50} values of 290.50 ± 9.12 nM (K_i = 265.17 ± 14.66 nM) for hCA I and IC_{50} value 177.03 ± 6.08 nM (K_i = 151.41 ± 3.29 nM) for hCA II Fig. 2.

When assessing the inhibition potential of compounds with various substitutions on the phenyl ring of TSC moiety, it was observed that nearly all derivatives showed significant inhibition compared with acetazolamide. For hCA I, compound **6 l** (IC_{50} = 88.43 ± 3.25 nM) was more potent due to presence of moderate electron-withdrawing chloro groups at *ortho* and *meta* positions. Compound **6 h** (IC_{50} = 108.60 ± 7.32 nM) exhibits higher inhibitory potential than **6f** (IC_{50} = 113.52 ± 4.35 nM) due to intramolecular attraction. Compound **6 t** (IC_{50} = 140.26 ± 5.91 nM) showed higher inhibitory potential compared to **6n** (IC_{50} = 146.05 ± 5.41 nM) owing to the presence of an electron donating substitution at the *meta* position. Compound **6n** (IC_{50} = 146.05 ± 5.41 nM) demonstrated a notably lower value compared to **6o** (IC_{50} = 179.92 ± 6.68 nM), indicating strong inhibitory potential likely due to the presence of electron-withdrawing NO_2 group at the *meta* position. Among the three compounds, **6j** (IC_{50} = 167.30 ± 5.22 nM) and **6i** (IC_{50} =

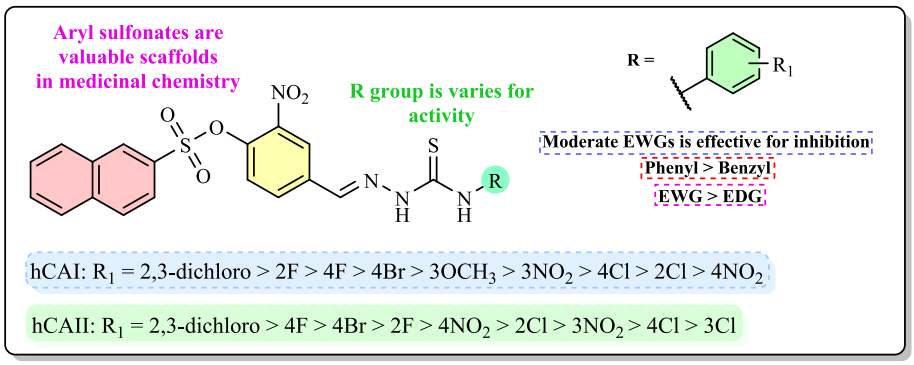

Fig. 2. SAR of the synthesized thiosemicarbazones.

174.51 ± 7.38 nM) exhibited the lowest value than **6 k** (IC_{50} = 189.78 ± 6.44 nM) due to the presence of chloro group at *para* and *ortho* positions, respectively. When examined **6d** possesses strongest inhibitory activity (IC_{50} = 212.05 ± 11.48 nM), than **6 g** (IC_{50} = 235.48 ± 7.23 nM) and **6e** (IC_{50} = 286.47 ± 8.13 nM) respectively. The compound **6q** (IC_{50} = 289.32 ± 7.59 nM) was found to be significantly potent as compared to **6r** (IC_{50} = 342.21 ± 9.19 nM) due to the presence of methyl groups at *ortho* and *para* positions. Compound **6p** (IC_{50} = 360.80 ± 6.05 nM) exhibited lower value than **6 s** (IC_{50} = 368.29 ± 10.71 nM), indicating higher potency because the methyl group at *ortho* position causes less steric hindrance. The enhanced activity of **6b** (IC_{50} = 247.09 ± 9.31 nM) compared to **6c** (IC_{50} = 380. 07 ± 8.32 nM) was likely due to a smaller methyl group causing minimal steric hindrance.

For hCA II, compound **6 l** (IC_{50} = 61.82 ± 0.60 nM) was more potent due to presence of moderate electron-withdrawing chloro groups at *ortho* and *meta* positions. Compound **6f** (IC_{50} = 82.82 ± 3.24 nM) exhibits higher inhibitory potential than **6 h** (IC_{50} = 93.16 ± 2.06 nM) due to presence of benzyl group. Compound **6o** (IC_{50} = 115.62 ± 1.39 nM) showed higher inhibitory potential compared to **6n** (IC_{50} = 123.40 ± 1.23 nM) due to strong electron withdrawing NO_2 substitution at *para* position. Compound **6 m** (IC_{50} = 85.12 ± 1.36 nM) exhibited lower value compared to **6j** (IC_{50} = 158.11 ± 4.30 nM), indicating strong inhibitory potential likely due to electronegative bromo substitution at *para* position. Among the three compounds, **6 g** (IC_{50} = 133.35 ± 2.77 nM) and **6e** (IC_{50} = 138.23 ± 2.38 nM) exhibited the lowest value than **6d** (IC_{50} = 152.38 ± 1.43 nM) due to the presence of phenyl and benzyl groups, respectively. The compound **6q** (IC_{50} = 147.35 ± 3.54 nM) was found to be significantly potent as compared to **6r** (IC_{50} = 170.24 ± 3.19 nM) due to the presence of methyl groups at *ortho* and *para* positions. Compound **6p** (IC_{50} = 275.25 ± 3.62 nM) exhibited lower value than **6 s** (IC_{50} = 277.37 ± 3.91 nM), indicating higher potency because the methyl group at *ortho* position causes less steric hindrance. The enhanced activity of **6b** (IC_{50} = 128.46 ± 2.29 nM) compared to **6c** (IC_{50} = 190.20 ± 5.38 nM) was likely due to a smaller methyl group causing minimal steric hindrance.

2.4. Metal chelating

Metal-chelating assay is an antioxidant method based on measuring the absorbance of the ferrous ion (Fe^{2+})-ferrozine complex after the addition of a test sample to a Fe^{2+} solution. The presence of antioxidant chelators is indicated by a reduction in the formation of the Fe^{2+}-ferrozine complex, as ferrozine only binds free Fe^{2+} ions, not those bound to other chelators. This reaction forms a red-colored chromophore with a measurable absorbance at 562 nm. However, a key limitation of this method is the competition between ferrozine and the test compounds for Fe^{2+} binding, along with differences in the stability of their respective Fe^{2+} complexes. This makes it difficult to accurately quantify weak iron chelators, as their chelating ability may be underestimated. Despite this, metal-chelating capacity is considered significant because it reduces the concentration of free transition metals that promote lipid peroxidation. Chelating agents are regarded as effective secondary antioxidants due to their ability to stabilize metals in their oxidized state and lower redox potential. In this study, EDTA was used as the reference chelator due to its strong metal-binding ability. As shown in Table 1, the novel compounds demonstrated significant iron-binding activity, which could be linked to their potential as lipid peroxidation inhibitors. The difference in activity between the control and varying concentrations (9 to 76 nM) of the tested compounds was statistically significant. Furthermore, the IC_{50} values of the novel compounds ranged from (9.43 ± 0.80 to 75.24 ± 8.35). In comparison, EDTA exhibited an IC_{50} value of 13.28 ± 0.98 nM. Notably, several compounds (**6 h:** 9.43 ± 0.80 nM, **6 l:** 10.86 ± 0.16 nM, **6n:** 11.14 ± 1.46 nM, and **6f:** 11.31 ± 0.57 nM) showed IC_{50} values lower than that of EDTA, suggesting strong metal chelating potential. The N (iminic nitrogen) and S (thione sulfur) atoms in 4-formyl-2-nitrophenyl naphthalene-2-sulfonate thiosemicarbazones usually form bidentate chelates with metal ions. Sulfonate oxygen can also be used to provide tridentate coordination when needed. After condensation with thiosemicarbazide, the molecule 4-formyl-2-nitrophenyl naphthalene-2-sulfonate yields a thiosemicarbazone derivative having the structure –CH=N–NH–C(*S*)NH_2 [54]. Resonance-stabilized thione–thiol tautomerism is present in this structure:

R–CH = N–NH–C(*S*)NH_2⇌R–CH = N–NH–C(–SH) = NH

The S atom can readily establish a connection with the metal ion when the thiol form (-SH) is present. There are several important donor atoms in the thiosemicarbazone structure. The synthesized ligand contains several functional groups that contribute differently to metal complexation. The C=NNH–C(*S*)NH_2 moiety serves as the main chelation center, with both the nitrogen (–C=NN–) and sulfur (C=S) atoms directly coordinating to the metal. The aldehyde group (–CHO) can participate indirectly by forming an imine nitrogen after condensation, which may also engage in coordination. The nitrophenyl group is generally passive, acting primarily as an electron-withdrawing group that reduces the electron density of the ligand without directly participating in binding. Finally, the naphthalene-sulfonate moiety ($–SO_3^-$) can form ionic or coordinative interactions, particularly with alkali or transition metal ions, further stabilizing the complex.

2.5. Computational studies

2.5.1. Docking of hCA I inhibitors

Most active inhibitors of hCA I and hCA II (**6f, 6 h, 6 l, 6 m** and **6n**) were selected for the docking studies. All compounds showed inhibition against both isozymes of *CA*. The crystal structures of hCA I and hCA II were downloaded from the PDB (PDB ids: 3lxe and 1a42). To validate the docking protocol, the co-crystallized ligand was extracted and docked into the enzyme, the docking conformation was able to reproduce the experimentally observed conformation of the ligand. All

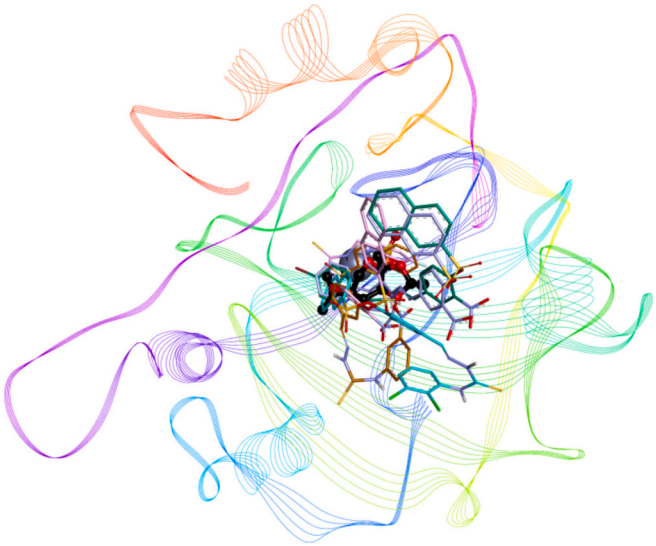

Fig. 3. Overlap of docked conformations of most active hCA I inhibitors **6f, 6 h, 6 l, 6 m** and **6n** in the active site with the co-crystallized inhibitor (represented in black).

inhibitors of hCA I were found to bind in the active site Fig. 3.

All compounds were found to have similar binding orientations in the active site near the zinc metal ion Fig. 4. Several recurring and potentially critical interactions that appear to contribute to binding affinity and specificity were observed Table 2. Among hydrogen bonded interactions, Gln92 was making hydrogen bonds with the NH groups of **6 h** and **6 m**, while His64 was making hydrogen bonds with the sulfone group oxygen atom of compound **6n** and with the nitrogen atom of **6 f**. In compounds **6f, 6 l** and **6n** His67 was making π-cation interactions with the nitro group.

The zinc metal ion of the active site was also making π-cation interaction with the phenyl ring of **6 h** and **6 m**, and with naphthyl ring of **6n**. In compounds **6f, 6 h, 6 l** and **6 m** His64 was involved in pi-donor interaction with the aromatic phenyl and naphthyl ring. Noncovalent pi-sulfur interactions were observed for compounds **6f, 6 l, 6 m** and **6n** with Hos64, His67 and His96.

One of the oxygen atoms of the nitro group of most active hCA I inhibitor **6 l** was making a π-cation bond with His67, while the other oxygen atom was making an intra-molecular pi-anion contact with the naphthalene ring. Two pi-sulfur bonds were observed between the sulfur atom of the sulfonate group and amino acids His67 and His64. The naphthalene ring was making pi-pi T-shaped contacts with His64 and His200.

The SAR analysis of hCA I inhibitors (6f–6n) reveals that the most potent derivatives (6 h, 6 m, 6n) share critical interactions with the catalytic zinc center and neighboring histidine residues (His64, His67, His94). The presence of halogen and sulfur substituents further enhances binding through halogen, pi-sulfur, and hydrophobic contacts. Compounds 6f and 6 l, lacked direct coordination with the zinc ion, instead pi-pi and pi-sulfur interactions were observed, this is in agreement with their comparatively moderate activity. These results rationalize the observed experimental inhibition activity and suggest that metal coordination, halogen bonding, and aromatic stacking mainly contributes to increased inhibitory activity against hCA I.

2.5.2. *Docking of hCA II inhibitors*

In general, no specificity towards over any one type of hCA isozyme (hCA I or hCA II) could be observed. In-fact, compound **6 l**, that was the most active hCA I inhibitor was also the most active inhibitor of hCA II. The docking studies indicated that all compounds bind in the same area of the active site as the co-crystallized inhibitor Fig. 5.

Among hydrogen bonded interactions, Asn62 and Asn67 were making hydrogen bonds with sulfone group oxygen in compounds **6f, 6 l** and **6 m**. Another amino acid Thr200 was involved in hydrogen bond formation with oxygen atoms of nitro groups of compounds **6f** and **6 m**. The pi-cation interactions observed in compounds **6f, 6 h, 6 l, 6 m, 6n** between the ligand's amine group with an aromatic or charged system also seemed to stabilize the orientation of the ligands in the binding site. Similarly pi-anion interactions in compounds **6f, 6 h, 6 l, 6 m** and **6n** involving intramolecular interactions between the electron-rich oxygen and a π-system were also deemed significant for stabilizing binding site interactions.

Pi-alkyl interactions are non-polar stabilizing interactions signifying hydrophobic pocket engagement. Most ligands were found to engage with Val121, Val135, Pro202, Leu198 to form pi-alkyl interactions, additionally compound 3 h was making pi-alkyl interactions with Lys170. Similarly pi-pi stacking and pi-pi T-shaped interactions were observed for most compounds with Phe131, Trp5 and His64 **Table S1**. The interaction of sulfonamide group with the zinc metal ion of the active site of carbonic anhydrase is well-known and indeed most significant. However, for compounds studied herein no direct interaction of sulfone group with the zinc metal ion was observed, nevertheless for compound **6n**, the terminal nitro group was in contact with the zinc metal ion Fig. 4.

2.6. *Molecular dynamics simulation*

2.6.1. *Molecular dynamics simulation studies of hCA I inhibitor*

The molecular dynamics simulation analyses revealed that **6 l** with hCA I for 150 ns showed the C-α RMSD value increased from 1.25 Å to 2.38 Å in the initial 53 ns, then decreased to around 1.7 Å till the 84 ns mark, then remained comparatively stable around 1.75 Å towards the end of the simulation. The **6 l**'s lig fit on protein RMSD value increased to around 7.5 Å in the initial 22 ns, then remained stable around 7.5 Å till the 48 ns mark, then the value spiked to around 12 Å till the **61** ns mark, then decreased again to around 7.5 Å and found to be stable till the completion of simulation studies. **6 l**'s lig fit lig RMSD increased up to 3.6 Å in the initial 65 ns, then remained stable around 3.6 Å till the end of the simulation period. Protein RMSF analysis showed that the majority of residues showed fluctuations less than 1.5 Å during the simulation, where relatively higher fluctuations were shown by the residues in the N-terminal region of the protein, with the highest value by *Leu 19* at 2.68 Å. The total percentage of secondary structure elements was 37.09 %, where alpha-helices were 9.22 % and beta-strands were 27.87 %. **6 l**'s Ligand RMSF analysis revealed that most atoms in the ligand showed values around 3 Å, where relatively higher values between 4 and 5 Å were expressed by sulfur of thiourea and some atoms of the dichlorobenzene and naphthalene moieties. Protein Ligand Contacts showed that *His 67* showed most interactions, with an interaction fraction around 0.8, and consisted mostly of water bridges and hydrophobic interactions Fig. 6. Ligand Protein Contacts showed that *His 67* exhibited Pi-Pi stacking interactions with the benzene of **6 l** at 52 %. **6 l**'s torsional profile analysis revealed that most rotatable bonds showed stable behavior, where some relatively higher dynamic torsional behavior was exhibited by bonds of the nitro group and the dichlorobenzene attachment Fig. 7.

2.6.2. *Molecular dynamics simulation studies of hCA II inhibitor*

MD simulation results showed the C-α RMSD value with hCA II for 150 ns for **6 l** increased in the initial 38 ns from 0.9 Å to around 2.1 Å and then the value remained relatively stable around 2.1 Å till the end of the simulation. The **6 l**'s lig fit on protein RMSD value remained around 3 Å in initial 84 ns except two transient dips to around 1.5 Å between 37 and 45 ns, then the value increased to around 5 Å and remained around 5.2 Å till 110 ns mark, then following a transient spike to about 9.2 Å, the value remained around 6.5 Å till the end of the simulation. **6 l**'s lig fit lig RMSD remained mostly around 1.6 Å, except increase to around 3.1 Å

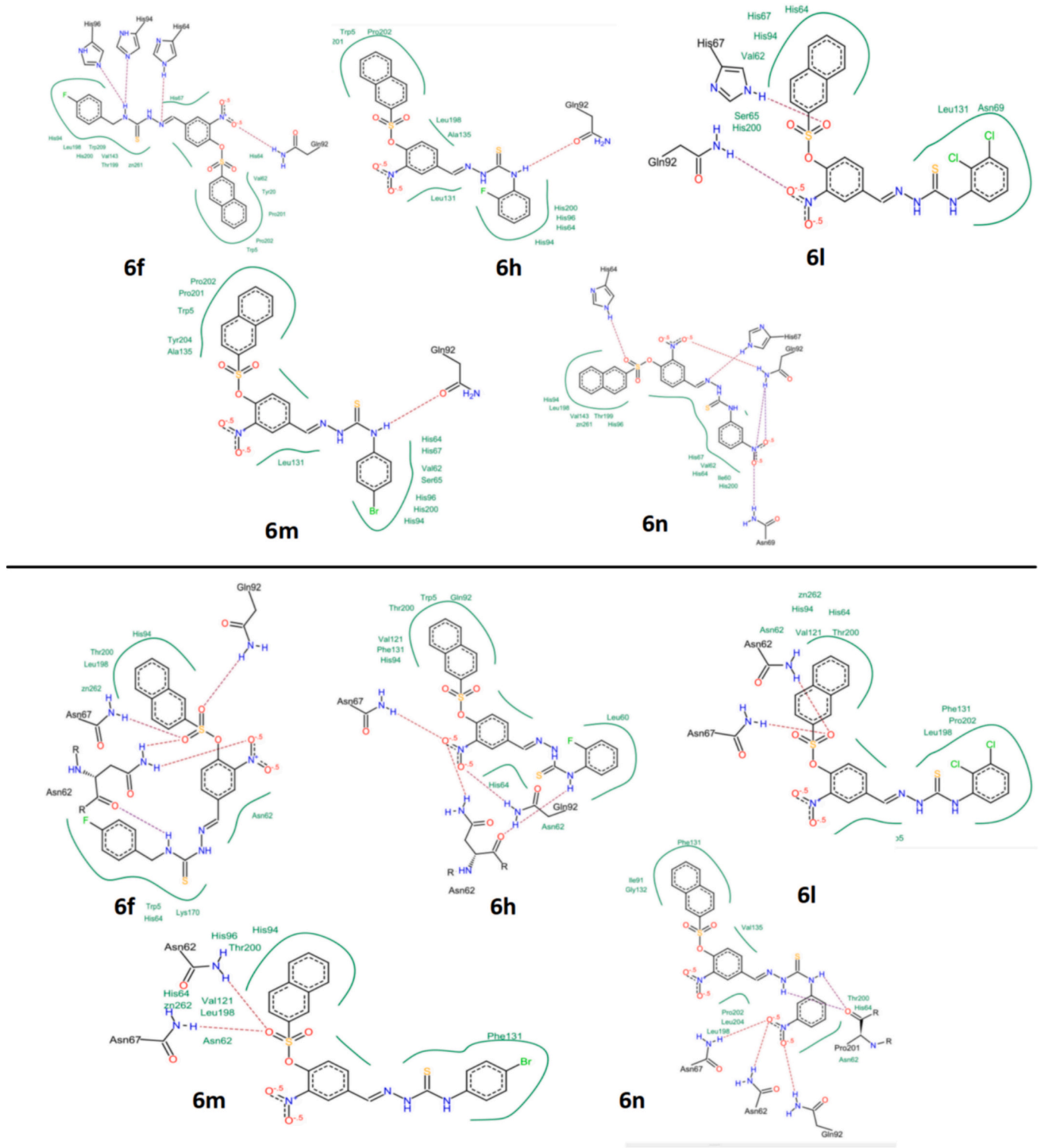

Fig. 4. Binding site interactions of docked conformations of compounds **6f**, **6 h**, **6 l**, **6 m**, and **6n**) against hCA I (top) and against hCA II (bottom).

between 98 and 111 ns. Protein's RMSF analysis revealed that the majority of residues showed values less than 2.5 Å, where relatively higher values were exhibited by residues in the N-terminal region. The total percentage of secondary structure elements was 32.86 %, where alpha-helices were 4.6 % and beta-strands were 28.26 %. **6 l**'s Ligand RMSF analysis revealed that the majority of atoms showed values less than 4 Å, where relatively higher values between 4 and 6 Å were expressed by sulfur of thiourea and some atoms of the dichlorobenzene and naphthalene moieties. Protein Ligand Contacts showed that His94 showed most interactions at around 1.2 interaction fraction and consisted mostly of water bridges and hydrophobic interactions Fig. 8. Ligand Protein Contacts showed that Gln92 maintained polar interaction at 58 % with sulfone group of **6 l**, while His94 maintained polar π-π stacking, and π-cation interactions with naphthalene moiety at 39 % and 70 % respectively, and Trp5 maintained π-π stacking interactions with dichlorobenzene moiety at 30 %. **6 l**'s torsional profile analysis showed

Table 2
Critical interactions of most active hCA I inhibitors **6f, 6 h, 6 l, 6 m** and **6n** that appear to contribute to binding affinity and specificity.

Code	Interactions	Type	Distance (Å)
6f	His64:He2 - Lig:N	Hydrogen bond	2.34
	Lig:C - Thr199:Og1	Carbon hydrogen bond	2.59
	Lig:N - His67	Pi-cation	3.96
	Thr199:Hn - Lig	Pi-donor	3.20
	Lig:S - Tyr7	Pi-Sulfur	5.02
	Lig:S - His64	Pi-Sulfur	5.38
	Lig:S - His96	Pi-Sulfur	3.67
	Lig - Trp5	Pi-pi stacked	4.87
	Lig - Trp5	Pi-pi stacked	5.03
	Trp5 - Lig	Pi-pi stacked	4.68
	His67 - Lig	Pi-pi stacked	4.79
	His94 - Lig	Pi-pi T-shaped	4.90
	Lig - Val143	Pi-alkyl	5.30
	Lig - Leu198	Pi-alkyl	4.63
	Lig - Pro202	Pi-alkyl	4.81
	Lig - Pro202	Pi-alkyl	3.91
6 h	Lig:H17 - Gln92:Oe1	Hydrogen bond	2.71
	Gln92:He22 - Lig:F1	Hydrogen bond;halogen (fluorine)	2.79
	His67:Cd2 - Lig:F1	Carbon hydrogen bond	3.17
	Zn261:Zn - Lig	Pi-cation	4.45
	His64:He2 - Lig	Pi-donor	3.03
	His94 - Lig	Pi-pi stacked	3.85
	Pro201:C,O;Pro202:N - Lig	Amide-pi stacked	4.50
	Lig - Pro202	Pi-alkyl	4.56
	Lig - Pro202	Pi-alkyl	3.89
6 l	Lig:N43 - Lig	Pi-cation	4.15
	Lig:N43 - His67	Pi-cation	4.81
	Lig:O45 - Lig	Pi-anion	3.97
	His64:He2 - Lig	Pi-donor	2.45
	Lig:S20 - His64	Pi-Sulfur	5.98
	Lig:S20 - His67	Pi-Sulfur	5.29
	His64 - Lig	Pi-pi T-shaped	4.46
	His64 - Lig	Pi-pi T-shaped	4.42
	His200 - Lig	Pi-pi T-shaped	5.41
	Lig - Val62	Pi-alkyl	4.84
	Lig - Val62	Pi-alkyl	5.32
6 m	Lig:H13 - Gln92:Oe1	Hydrogen bond	2.98
	Ala132:Ca - Lig:O48	Carbon hydrogen bond	3.11
	Zn261:Zn - Lig	Pi-cation	4.68
	His64:He2 - Lig	Pi-donor	2.95
	Lig:S11 - His64	Pi-Sulfur	5.83
	His94 - Lig	Pi-pi stacked	3.86
	His64 - Lig	Pi-pi T-shaped	4.95
	Pro201: C, O; Pro202: N - Lig	Amide-pi stacked	4.71
	Lig - Pro202	Pi-alkyl	4.36
	Lig - Pro202	Pi-alkyl	3.91
	Tyr7 - Lig:Br1	Pi-alkyl	5.31
	His64 - Lig:Br1	Pi-alkyl	4.45
	His96 - Lig:Br1	Pi-alkyl	3.96
6n	Lig:N2 - Lig:O55	Attractive charge	3.24
	Lig:N53 - Lig:O3	Attractive charge	4.37
	His64:He2 - Lig:O31	Hydrogen bond	2.14
	Gln92:He22 - Lig:O54	Hydrogen bond	1.76
	Arg173:Hh21 - Lig:S17	Hydrogen bond	2.70
	Lig:N53 - His67	Pi-cation	4.18
	Zn261:Zn - Lig	Pi-cation	3.24
	Lig:O3 - Lig	Pi-anion	3.78
	Lig:O55 - His67	Pi-anion	4.62
	Leu198:Cd2 - Lig	Pi-sigma	3.80
	Lig:S30 - His64	Pi-Sulfur	4.90
	Lig - Lig	Pi-pi stacked	5.37
	His67 - Lig	Pi-pi T-shaped	4.69
	Lig - Val62	Pi-alkyl	4.44
	Lig - Leu198	Pi-alkyl	5.43
	Lig - Ala121	Pi-alkyl	5.29
	Lig - Val143	Pi-alkyl	4.89

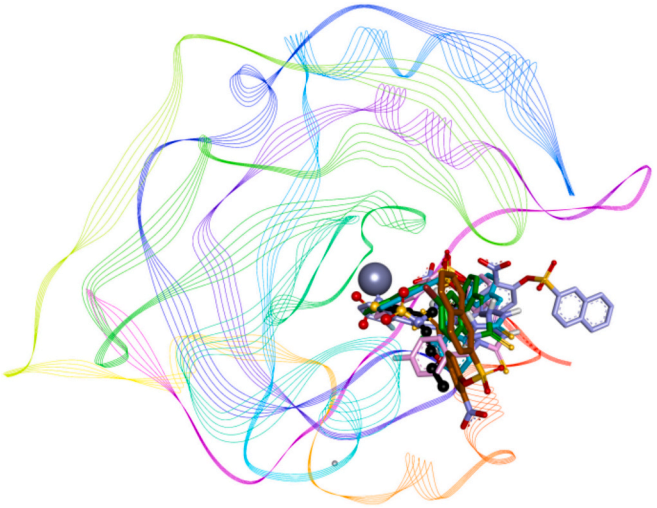

Fig. 5. Overlap of docked conformations of most active hCA II inhibitors **6f, 6 h, 6 l, 6 m** and **6n** in the active site with the co-crystallized inhibitor (represented in black).

that most rotatable bonds remained stable during simulation, where relatively higher torsional behavior was displayed by bonds of the nitro group and the dichlorobenzene attachment Fig. 9.

In molecular dynamics simulation studies of **6 l** with hCA I and hCA II, it was observed that both complexes remained relatively stable during the respective simulations, as the protein RMSDs in both complexes remained below 2.5 Å and showed stability. The compound **6 l** in both simulations, though it exhibited some movements in the first part of the respective simulations, however, seemed to have established a stable pose in both respective complexes towards the end of the simulations in both isozymes. In both simulations, it appeared that the sulfone moiety of **6 l** seems to prefer its orientation towards the central zinc metal ion in both respective complexes. Moreover, the commonality includes the higher RMSF of the N-terminal residues of both proteins, and similar **6 l**'s behavior in orientation, RMSF, and torsional dynamics in both simulations. Overall, both complexes seemed to have established equilibrium as both protein and ligand RMSD values plateaued towards the end in both simulations, indicating stability, which was also corroborated by the stable pose of **6 l** in both complexes to the end of the respective simulations.

2.7. In-silico prediction of ADME properties

In order to predict drug-likeness of compounds, ADME properties Swiss ADME was used. The results are given in **Table S2**.

Most compounds had molecular weights on the higher end (500–585), only compounds **6a-c** had molecular weights less than 500. The number of rotatable bonds was also high 7–10, indicating high molecular flexibility which may lead to decreased membrane permeability and oral bioavailability, which is evident from low gastrointestinal absorption (GI). The number of hydrogen bond donors and acceptors was well within the acceptable range (HBA $\leq$ 10, HBD $\leq$ 5). Topological polar surface area (PTSA) of all compounds was higher than ideal value of 140, indicating limiting membrane permeability, which is reaffirmed by inability of all compounds to cross blood brain barrier (BBB). Except **6a**, all compounds were predicted to be poorly water soluble. Although the ADME predictions indicate relatively low aqueous solubility for the synthesized thiosemicarbazones, their octanol–water partition coefficients are within favorable ranges, reflecting balanced lipophilicity. Low solubility is common for organic molecules of this type, and it can potentially be overcome using appropriate formulation strategies, including salt formation or suitable excipients, to improve

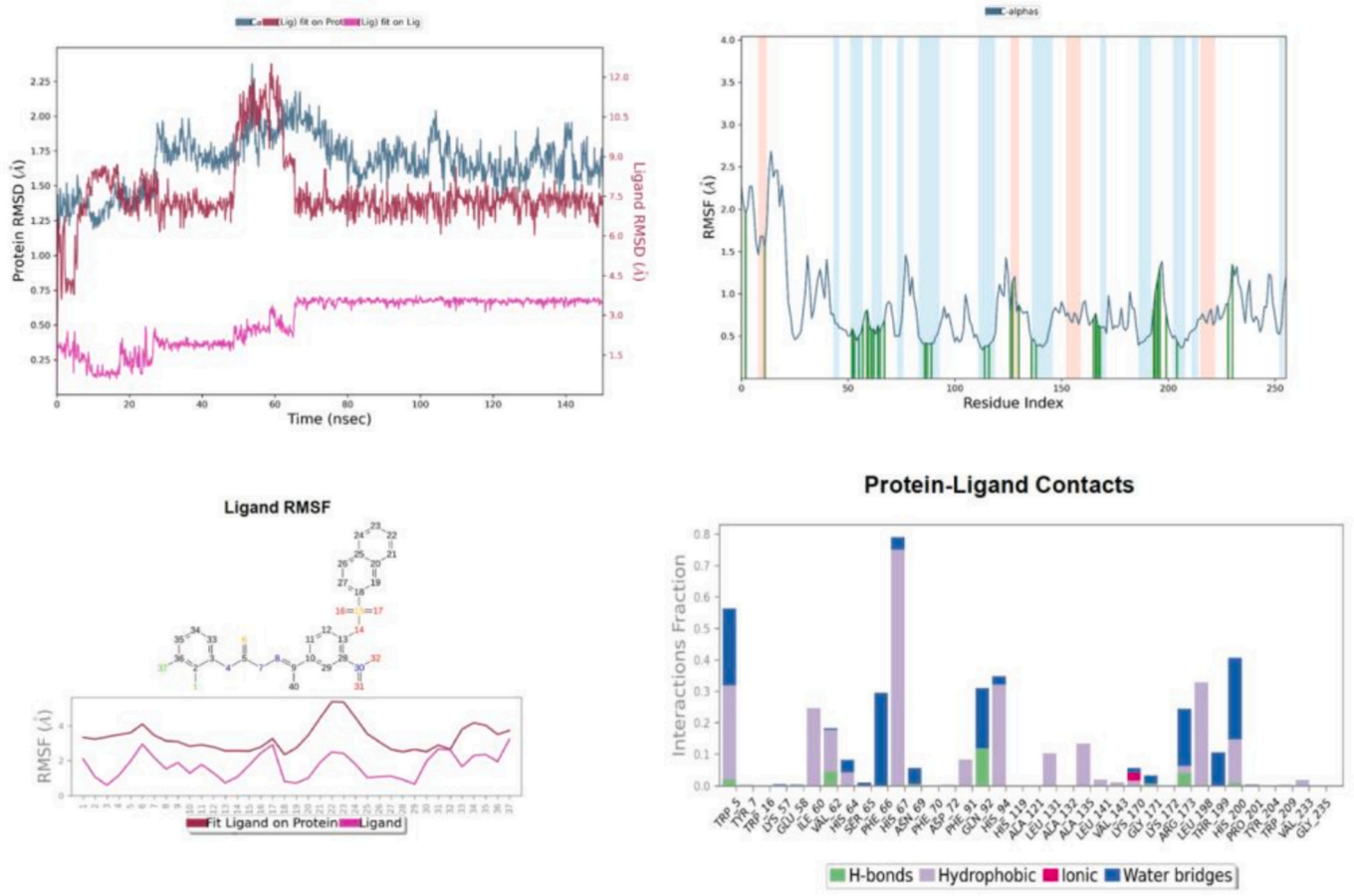

Fig. 6. MD simulation studies of complex of **6 l** with hCA I for 150 ns, RMSD plot; Protein RMSF graph; Ligand RMSF graph and protein ligand contacts.

bioavailability in therapeutic applications.

3. Experimental section

3.1. Chemistry

All chemicals required for the synthesis of 4-formyl-2-nitrophenyl naphthalene-2-sulfonate-derived thiosemicarbazones were obtained from Sigma-Aldrich. Petroleum ether, ethyl acetate, glacial acetic acid, nitric acid, dimethylformamide, ethanol and methanol were purchased from Merck and used in its original form. Aluminum-backed silica plates were utilized to monitor the completion of reaction. ^{1}H and ^{13}C NMR spectra were recorded at 25 °C using a Bruker Ascend 400 MHz NMR spectrometer, deuterated solvent such as DMSO-d_6 (400 MHz for ^{1}H and 100 MHz for ^{13}C NMR). Chemical shift (ppm) was used to represent the NMR spectra and coupling constant (*j*) were expressed in hertz (Hz) to describe the multiplicity of the signals.

3.2. Synthesis of 4-hydroxy-3-nitrobenzaldehyde (2)

4-Hydroxy-3-nitrobenzaldehyde **(2)** was synthesized by following a previously reported method [55]. 4-Hydroxybenzaldehyde **(1)** (1 mmol) was added to 10 mL of DCM, followed by the dropwise addition of nitric acid (HNO_3) (1 mmol). The mixture was sonicated for 30 min. The progress of the reaction was monitored by thin layer chromatography, and the formation of yellow precipitates indicated the completion of the reaction. The product was filtered and washed with water.

3.3. Synthesis of 4-formyl-2-nitrophenyl naphthalene-2-sulfonate (4)

4-Formyl-2-nitrophenyl naphthalene-2-sulfonate **(4)** was prepared by following reported method [55]. 4-Hydroxy-3-nitrobenzaldehyde **(2)** (3.425 mmol) and triethylamine (3.425 mmol) were dissolved in 10 mL of DMF, and the mixture was stirred in an ice bath. Naphthalene-2-sulphonyl chloride **(3)** (3.425 mmol) was added to the solution. The reaction mixture was examined by thin layer chromatography, and after 60 min, the reaction was quenched by adding distilled water (20 mL), resulting in the precipitation of the product. The precipitate was filtered, washed with ice cold water, dried at room temperature, and prepared for further analysis.

3.4. Synthesis of thiosemicarbazones 6(a-t)

Equimolar amounts of 4-formyl-2-nitrophenyl naphthalene-2-sulfonate **(4)** and thiosemicarbazides **5(a-t)** were dissolved in methanol, 3–4 drops of acetic acid were added as a catalyst and refluxed at 65–70 °C for 2–3 h. The reaction progress was examined by thin layer chromatography. Upon completion, the mixture was subjected to filtration, washed with methanol and dried at room temperature. The resulting compounds were characterized as follow:

(*E*)-4-[(2-Carbamothioylhydrazineylidene)methyl]-2-nitrophenyl naphthalene-2-sulfonate (6a)

Yellow solid, m.p. 231–233 °C, Yield 84 %. ^{1}H NMR (400 MHz, DMSO-d_6) δ 11.66 (s, 1H), 8.60 (d, $J = 2.0$ Hz, 1H), 8.57 (d, $J = 2.1$ Hz, 1H), 8.34 (s, 1H), 8.30–8.23 (m, 3H), 8.15 (d, $J = 8.2$ Hz, 1H), 8.08–8.03 (m, 2H), 7.83 (m, 2H), 7.74 (m, 1H), 7.20 (d, $J = 8.6$ Hz, 1H). ^{13}C NMR (100 MHz, DMSO-d_6) δ 178.9, 143.9, 140.5, 138.8, 135.8, 135.4, 133.4, 131.9, 131.3, 130.8, 130.8, 130.7, 130.3, 128.7, 128.5, 125.4, 124.0,

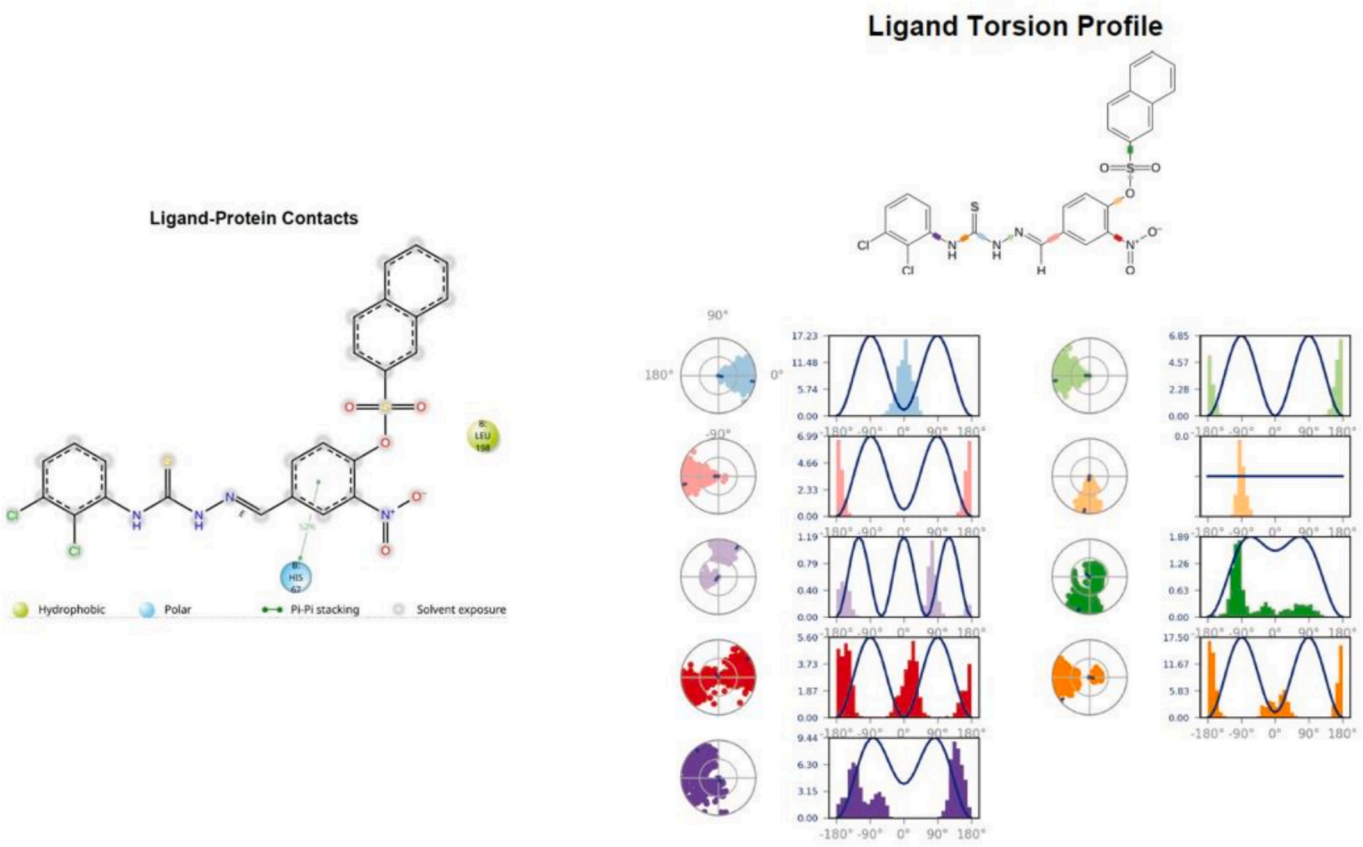

Fig. 7. Ligand Protein Contacts, and Ligand Torsion Profile of **6 l** with hCA I.

122.7.

(*E*)-4-{[2-(Methylcarbamothioyl)hydrazineylidene]methyl}-2-nitrophenyl naphthalene-2-sulfonate (6b)

Yellow solid, m.p. 218–220 °C, Yield 86 %. ^{1}H NMR (400 MHz, DMSO-d_6) δ 11.73 (s, 1H), 8.70 (q, J = 4.5 Hz, 1H), 8.61 (d, J = 2.0 Hz, 1H), 8.51 (d, J = 2.1 Hz, 1H), 8.25 (dd, J = 8.5, 5.7 Hz, 2H), 8.15 (d, J = 8.2 Hz, 1H), 8.09–8.03 (m, 2H), 7.87–7.80 (m, 2H), 7.74 (m, 1H), 7.21 (d, J = 8.6 Hz, 1H), 3.01 (d, J = 4.5 Hz, 3H). ^{13}C NMR (100 MHz, DMSO-d_6) δ 178.4, 143.9, 140.5, 138.3, 135.8, 135.5, 133.2, 131.9, 131.3, 130.9, 130.8, 130.7, 130.3, 128.7, 128.5, 125.5, 123.9, 122.7, 31.3.

(*E*)-4-{[2-(sec-Butylcarbamothioyl)hydrazineylidene]methyl}-2-nitrophenyl naphthalene-2-sulfonate (6c)

Yellow solid, m.p. 222–224 °C, Yield 79 %. ^{1}H NMR (400 MHz, DMSO-d_6) δ 11.69 (s, 1H), 8.72 (t, J = 6.0 Hz, 1H), 8.61 (d, J = 1.9 Hz, 1H), 8.48 (d, J = 2.1 Hz, 1H), 8.26 (dd, J = 8.5, 5.5 Hz, 2H), 8.15 (dd, J = 8.3, 1.2 Hz, 1H), 8.12 (dd, J = 8.6, 2.1 Hz, 1H), 8.07 (s, 1H), 7.87–7.81 (m, 2H), 7.75 (m, 1H), 7.22 (d, J = 8.6 Hz, 1H), 3.40 (t, J = 6.6 Hz, 2H), 2.02 (m, 1H), 0.89 (s, 3H), 0.87 (s, 3H). ^{13}C NMR (100 MHz, DMSO-d_6) δ 177.9, 143.8, 140.6, 138.5, 135.8, 135.4, 133.1, 131.9, 131.3, 130.8, 130.8, 130.7, 130.3, 128.7, 128.5, 125.4, 124.1, 122.7, 51.3, 28.3, 20.5.

(*E*)-4-{[2-(Cyclohexylcarbamothioyl)hydrazineylidene]methyl}-2-nitrophenyl naphthalene-2-sulfonate (6d)

Yellow solid, m.p. 234–236 °C, Yield 76 %. ^{1}H NMR (400 MHz, DMSO-d_6) δ 11.65 (s, 1H), 8.61 (d, J = 2.0 Hz, 1H), 8.42 (d, J = 2.1 Hz, 1H), 8.26 (dd, J = 8.5, 5.8 Hz, 2H), 8.19–8.13 (m, 3H), 8.07 (s, 1H), 7.85 (dd, J = 3.2, 1.7 Hz, 1H), 7.84–7.81 (m, 1H), 7.75 (m, 1H), 7.21 (d, J = 8.6 Hz, 1H), 4.24–4.12 (m, 1H), 1.86 (dd, J = 11.9, 3.9 Hz, 2H), 1.73 (m, 2H), 1.61 (d, J = 12.4 Hz, 1H), 1.40 (m, 2H), 1.27 (m, 2H), 1.11 (m, 1H). ^{13}C NMR (100 MHz, DMSO-d_6) δ 176.4, 143.8, 140.6, 138.8, 135.8, 135.2, 133.1, 131.9, 131.3, 130.9, 130.8, 130.7, 130.3, 128.7, 128.5, 125.4, 124.4, 122.7, 53.4, 32.1, 25.6, 25.4.

(*E*)-4-{[2-(Benzylcarbamothioyl)hydrazineylidene]methyl}-2-nitrophenyl naphthalene-2-sulfonate (6e)

Yellow solid, m.p. 215–217 °C, Yield 81 %. ^{1}H NMR (400 MHz, DMSO-d_6) δ 11.86 (s, 1H), 9.28 (t, J = 6.3 Hz, 1H), 8.60 (d, J = 2.0 Hz, 1H), 8.51 (d, J = 2.1 Hz, 1H), 8.25 (dd, J = 8.5, 4.8 Hz, 2H), 8.15–8.08 (m, 3H), 7.85–7.80 (m, 2H), 7.76–7.71 (m, 1H), 7.32 (d, J = 4.4 Hz, 4H), 7.24 (p, J = 4.6 Hz, 1H), 7.19 (d, J = 8.6 Hz, 1H), 4.85 (d, J = 6.2 Hz, 2H). ^{13}C NMR (100 MHz, DMSO-d_6) δ 178.4, 143.8, 140.6, 139.6, 138.9, 135.8, 135.4, 133.3, 131.9, 131.3, 130.9, 130.8, 130.7, 130.3, 128.7, 128.6, 128.5, 127.5, 127.2, 125.4, 124.1, 122.7, 47.0.

(*E*)-4-{[2-((4-Fluorobenzyl)carbamothioyl)hydrazineylidene]methyl}-2-nitrophenyl naphthalene-2-sulfonate (6f)

Yellow solid, m.p. 208–210 °C, Yield 85 %. ^{1}H NMR (400 MHz, DMSO-d_6) δ 11.88 (s, 1H), 9.29 (t, J = 6.3 Hz, 1H), 8.61 (d, J = 1.9 Hz, 1H), 8.51 (d, J = 2.1 Hz, 1H), 8.27–8.23 (m, 2H), 8.16–8.11 (m, 2H), 8.10 (d, J = 2.2 Hz, 1H), 7.86–7.80 (m, 2H), 7.74 (m, 1H), 7.39–7.34 (m, 2H), 7.20 (d, J = 8.6 Hz, 1H), 7.18–7.13 (m, 2H), 4.82 (d, J = 6.2 Hz, 2H). ^{13}C NMR (100 MHz, DMSO-d_6) δ 178.3, 162.8 ($J^{1}_{C\text{-}F}$ = 243.17 Hz), 143.8, 140.7, 139.0, 135.8, 135.8, 135.7, 135.3, 133.3, 131.9, 131.3, 130.8, 130.8, 130.7, 130.3, 129.5, 129.4, 128.7, 128.5, 125.4, 124.1, 122.7, 115.4, 115.2, 46.3.

(*E*)-2-Nitro-4-{[2-(Phenylcarbamothioyl)hydrazineylidene]methyl}phenyl naphthalene-2-sulfonate (6 g)

Yellow solid, m.p. 228–230 °C, Yield 75 %. ^{1}H NMR (400 MHz, DMSO-d_6) δ 12.06 (s, 1H), 10.27 (s, 1H), 8.62 (dd, J = 5.1, 2.0 Hz, 2H), 8.26 (dd, J = 8.4, 4.6 Hz, 2H), 8.20–8.12 (m, 3H), 7.83 (m, 2H), 7.74 (m, 1H), 7.51–7.47 (m, 2H), 7.38 (t, J = 7.9 Hz, 2H), 7.23 (t, J = 8.2 Hz, 2H). ^{13}C NMR (100 MHz, DMSO-d_6) δ 177.0, 143.9, 140.7, 139.4, 139.3, 135.8, 135.2, 133.7, 131.9, 131.3, 130.9, 130.8, 130.7, 130.3, 128.7, 128.6, 128.5, 126.9, 126.2, 125.4, 124.3, 122.7.

(*E*)-4-{[2-((2-Fluorophenyl)carbamothioyl)hydrazineylidene]methyl}-2-nitrophenyl naphthalene-2-sulfonate (6 h)

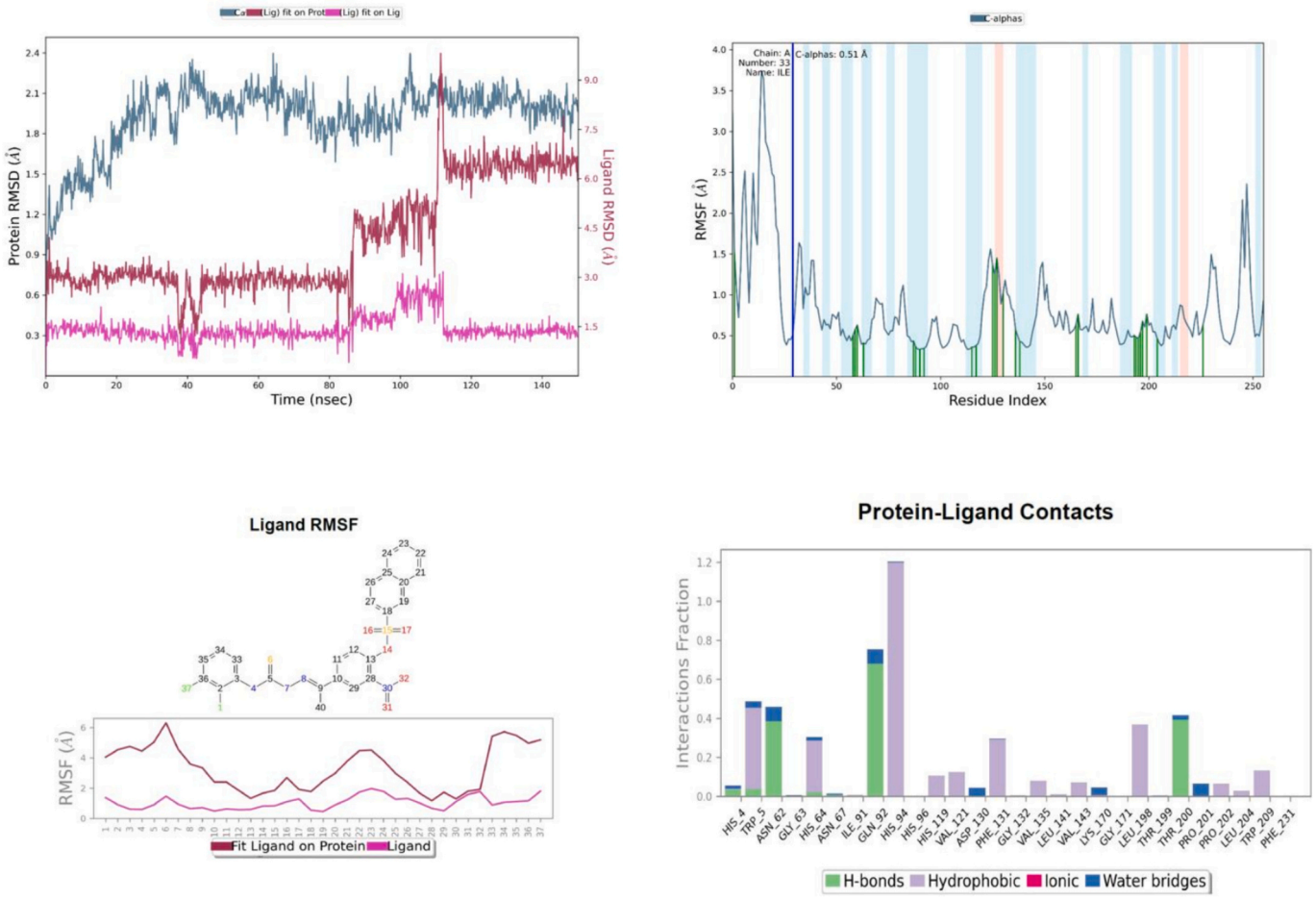

Fig. 8. MD simulation studies of complex of **6 l** with hCA II for 150 ns, RMSD plot; Protein RMSF graph; Ligand RMSF graph and protein ligand contacts.

Yellow solid, m.p. 212–214 °C, Yield 79 %. ^{1}H NMR (400 MHz, DMSO-d_6) δ 12.20 (s, 1H), 10.12 (s, 1H), 8.62 (dd, J = 6.7, 2.0 Hz, 2H), 8.25 (dd, J = 8.4, 3.7 Hz, 2H), 8.16 (d, J = 4.3 Hz, 2H), 8.14 (t, J = 2.2 Hz, 1H), 7.86–7.80 (m, 2H), 7.74 (m, 1H), 7.43 (m, 1H), 7.39–7.33 (m, 1H), 7.32–7.28 (m, 1H), 7.27–7.20 (m, 2H). ^{13}C NMR (100 MHz, DMSO-d_6) δ 178.3, 159.30 ($J^{l}_{C\text{-}F}$ = 248.03 Hz), 143.9, 140.8, 139.7, 135.8, 135.2, 133.8, 131.9, 131.3, 131.1, 130.9, 130.8, 130.7, 130.3, 128.7, 128.5, 125.5, 124.6, 124.6, 124.2, 122.7, 116.3, 116.1.

(*E*)-4-{[2-((2-Chlorophenyl)carbamothioyl)hydrazineylidene] methyl}-2-nitrophenyl naphthalene-2-sulfonate (6i)

Yellow solid, m.p. 219–221 °C, Yield 80 %. ^{1}H NMR (400 MHz, DMSO-d_6) δ 12.20 (s, 1H), 10.25 (s, 1H), 8.64 (d, J = 2.1 Hz, 1H), 8.61 (d, J = 2.0 Hz, 1H), 8.27 (d, J = 4.3 Hz, 1H), 8.25 (d, J = 3.6 Hz, 1H), 8.16–8.14 (m, 2H), 8.13 (d, J = 2.1 Hz, 1H), 7.83 (m, 2H), 7.74 (m, 1H), 7.55 (m, 2H), 7.37 (m, 2H), 7.23 (d, J = 8.6 Hz, 1H). ^{13}C NMR (100 MHz, DMSO-d_6) δ 177.9, 143.9, 140.8, 139.6, 137.0, 135.8, 135.2, 133.8, 132.0, 131.9, 131.3, 131.2, 130.9, 130.8, 130.7, 130.3, 129.8, 128.8, 128.7, 128.5, 127.7, 125.5, 124.1, 122.7.

(*E*)-4-{[2-((4-Chlorophenyl)carbamothioyl)hydrazineylidene] methyl}-2-nitrophenyl naphthalene-2-sulfonate (6j)

Yellow solid, m.p. 229–231 °C, Yield 84 %. ^{1}H NMR (400 MHz, DMSO-d_6) δ 12.14 (s, 1H), 10.28 (s, 1H), 8.61 (d, J = 2.0 Hz, 2H), 8.25 (dd, J = 8.5, 5.3 Hz, 2H), 8.20–8.13 (m, 3H), 7.87–7.80 (m, 2H), 7.74 (m, 1H), 7.56–7.52 (m, 2H), 7.45–7.41 (m, 2H), 7.23 (d, J = 8.6 Hz, 1H). ^{13}C NMR (100 MHz, DMSO-d_6) δ 177.0, 143.9, 140.8, 139.8, 138.3, 135.8, 135.1, 133.7, 131.9, 131.3, 130.9, 130.8, 130.7, 130.3, 130.2, 128.7, 128.5, 128.4, 125.4, 124.4, 122.7.

(*E*)-4-{[2-((3-Chlorophenyl)carbamothioyl)hydrazineylidene] methyl}-2-nitrophenyl naphthalene-2-sulfonate (6 k)

Yellow solid, m.p. 228–230 °C, Yield 86 %. ^{1}H NMR (400 MHz, DMSO-d_6) δ 12.19 (s, 1H), 10.30 (s, 1H), 8.61 (t, J = 1.7 Hz, 2H), 8.26 (dd, J = 8.5, 5.4 Hz, 2H), 8.20 (dd, J = 8.7, 2.1 Hz, 1H), 8.18–8.13 (m, 2H), 7.87–7.80 (m, 2H), 7.74 (m, 1H), 7.67 (t, J = 2.0 Hz, 1H), 7.55–7.50 (m, 1H), 7.41 (t, J = 8.0 Hz, 1H), 7.29 (m, 1H), 7.24 (d, J = 8.6 Hz, 1H). ^{13}C NMR (100 MHz, DMSO-d_6) δ 176.8, 143.9, 140.8, 140.8, 140.0, 135.8, 135.0, 133.7, 132.6, 131.9, 131.3, 130.9, 130.8, 130.7, 130.3, 130.1, 128.7, 128.5, 126.2, 125.8, 125.4, 125.2, 124.5, 122.7.

(*E*)-4-{[2-((2,3-Dichlorophenyl)carbamothioyl)hydrazineylidene] methyl}-2-nitrophenyl naphthalene-2-sulfonate (6 l)

Yellow solid, m.p. 160–162 °C, Yield 83 %. ^{1}H NMR (400 MHz, DMSO-d_6) δ 12.28 (s, 1H), 10.32 (s, 1H), 8.63 (d, J = 2.1 Hz, 1H), 8.61 (d, J = 2.0 Hz, 1H), 8.27 (d, J = 4.5 Hz, 1H), 8.24 (d, J = 3.8 Hz, 1H), 8.17–8.15 (m, 2H), 8.13 (d, J = 1.9 Hz, 1H), 7.87–7.80 (m, 2H), 7.74 (m, 1H), 7.62 (dd, J = 8.0, 1.6 Hz, 1H), 7.52 (dd, J = 8.0, 1.6 Hz, 1H), 7.41 (t, J = 8.0 Hz, 1H), 7.23 (d, J = 8.6 Hz, 1H). ^{13}C NMR (100 MHz, DMSO-d_6) δ 177.9, 143.9, 140.8, 139.9, 139.1, 135.8, 135.1, 133.8, 132.2, 131.9, 131.3, 131.0, 130.9, 130.8, 130.7, 130.3, 130.1, 129.3, 128.7, 128.5, 128.2, 125.5, 124.2, 122.7.

(*E*)-4-{[2-((4-Bromophenyl)carbamothioyl)hydrazineylidene] methyl}-2-nitrophenyl naphthalene-2-sulfonate (6 m)

Yellow solid, m.p. 227–229 °C, Yield 80$^{o}/_{o}$. ^{1}H NMR (400 MHz, DMSO-d_6) δ 12.15 (s, 1H), 10.27 (s, 1H), 8.61 (d, J = 2.0 Hz, 2H), 8.26 (dd, J = 8.5, 5.3 Hz, 2H), 8.20–8.15 (m, 2H), 8.14 (s, 1H), 7.87–7.80 (m, 2H), 7.74 (m, 1H), 7.59–7.54 (m, 2H), 7.52–7.47 (m, 2H), 7.23 (d, J = 8.6 Hz, 1H). ^{13}C NMR (100 MHz, DMSO-d_6) δ 176.9, 143.9, 140.8, 139.8, 138.7, 135.8, 135.1, 133.7, 131.9, 131.4, 131.3, 130.9, 130.8, 130.7, 130.3, 128.7, 128.7, 128.5, 125.4, 124.4, 122.7, 118.4.

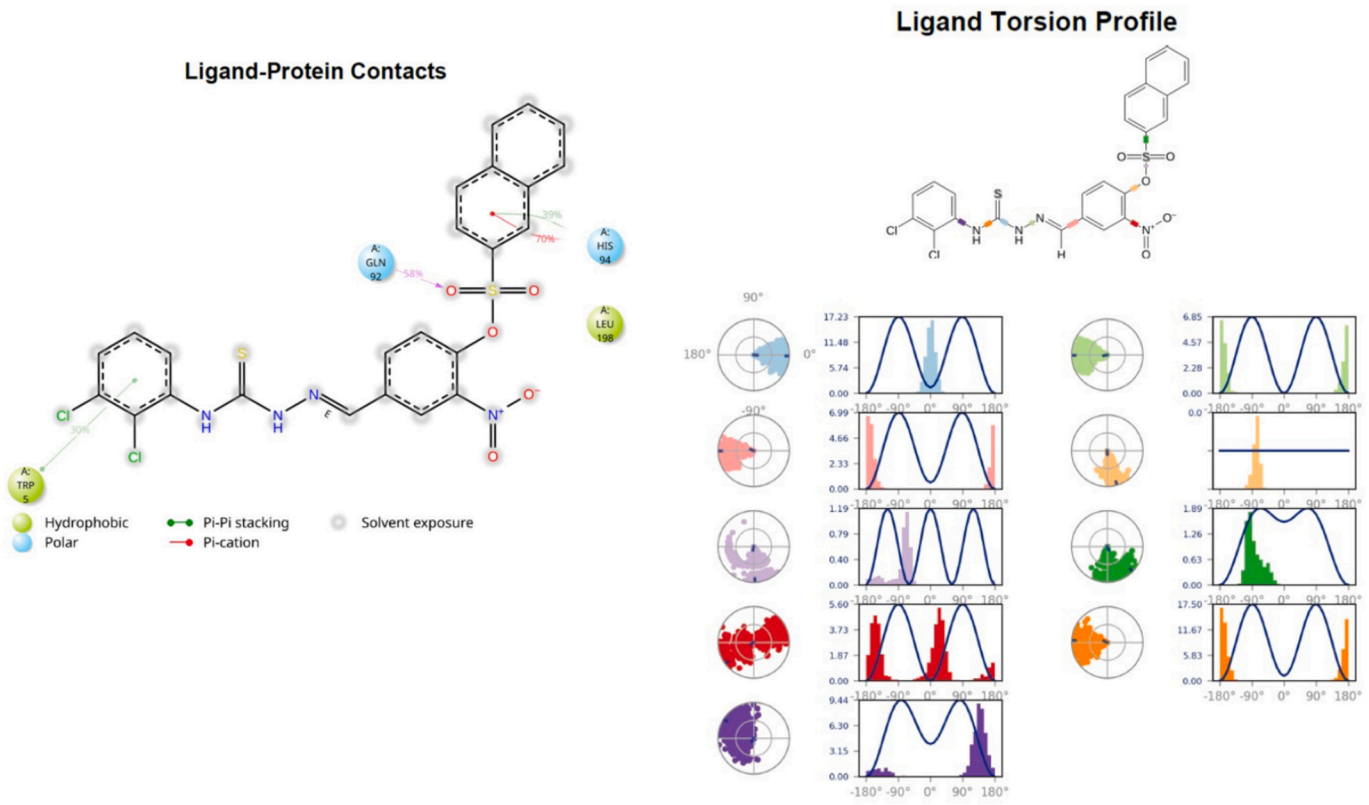

Fig. 9. Ligand Protein Contacts, and Ligand Torsion Profile of **6 l** with hCA II.

(*E*)-2-Nitro-4-{[2-((3-Nitrophenyl)carbamothioyl)hydrazineylidene]methyl}phenyl naphthalene-2-sulfonate (6n)

Yellow solid, m.p. 236–238 °C, Yield 81 %. ^{1}H NMR (400 MHz, DMSO-d_6) δ 12.33 (s, 1H), 10.50 (s, 1H), 8.62 (d, J = 2.1 Hz, 2H), 8.55 (t, J = 2.2 Hz, 1H), 8.28–8.25 (m, 2H), 8.24 (dd, J = 2.8, 1.6 Hz, 1H), 8.21 (d, J = 3.8 Hz, 1H), 8.18–8.12 (m, 1H), 8.11–8.04 (m, 2H), 7.84 (m, 2H), 7.75 (m, 1H), 7.67 (t, J = 8.2 Hz, 1H), 7.26 (d, J = 8.6 Hz, 1H). ^{13}C NMR (100 MHz, DMSO-d_6) δ 176.9, 147.7, 143.8, 140.9, 140.5, 140.5, 135.8, 134.9, 133.8, 132.7, 131.9, 131.3, 130.9, 130.8, 130.7, 130.3, 129.8, 128.7, 128.5, 125.5, 124.6, 122.7, 120.6, 120.5.

(*E*)-2-Nitro-4-{[2-((4-Nitrophenyl)carbamothioyl)hydrazineylidene]methyl}phenyl naphthalene-2-sulfonate (6o)

Yellow solid, m.p. 221–223 °C, Yield 85 %. ^{1}H NMR (400 MHz, DMSO-d_6) δ 12.40 (s, 1H), 10.53 (s, 1H), 8.62 (t, J = 1.7 Hz, 2H), 8.28–8.23 (m, 5H), 8.22 (d, J = 2.3 Hz, 1H), 8.17–8.13 (m, 1H), 8.02–7.98 (m, 2H), 7.84 (m, 2H), 7.75 (m, 1H), 7.27 (d, J = 8.6 Hz, 1H). ^{13}C NMR (100 MHz, DMSO-d_6) δ 176.3, 145.6, 144.2, 143.8, 141.0, 140.7, 135.8, 134.8, 133.8, 131.9, 131.3, 130.9, 130.8, 130.7, 130.3, 128.7, 128.5, 125.5, 124.7, 124.2, 122.7.

(*E*)-2-Nitro-4-{[2-(o-Tolylcarbamothioyl)hydrazineylidene]methyl}phenyl naphthalene-2-sulfonate (6p)

Yellow solid, m.p. 242–244 °C, Yield 84 %. ^{1}H NMR (400 MHz, DMSO-d_6) δ 12.03 (s, 1H), 10.15 (s, 1H), 8.66 (d, J = 2.1 Hz, 1H), 8.61 (d, J = 2.0 Hz, 1H), 8.28–8.24 (m, 2H), 8.16–8.14 (m, 2H), 8.13 (t, J = 2.0 Hz, 1H), 7.83 (m, 2H), 7.74 (m, 1H), 7.30–7.26 (m, 1H), 7.24–7.20 (m, 4H), 2.21 (s, 3H). ^{13}C NMR (100 MHz, DMSO-d_6) δ 177.7, 143.9, 140.6, 139.0, 138.4, 136.2, 135.8, 135.4, 133.7, 131.9, 131.3, 130.8, 130.8, 130.7, 130.5, 130.3, 129.4, 128.7, 128.5, 127.4, 126.5, 125.4, 124.0, 122.7, 18.2.

(*E*)-4-{[2-((2,4-Dimethylphenyl)carbamothioyl)hydrazineylidene]methyl}-2-nitrophenyl naphthalene-2-sulfonate (6q)

Yellow solid, m.p. 233–235 °C, Yield 77 %. ^{1}H NMR (400 MHz, DMSO-d_6) δ 11.98 (s, 1H), 10.07 (s, 1H), 8.63 (dd, J = 13.9, 2.0 Hz, 2H), 8.25 (dd, J = 8.5, 3.5 Hz, 2H), 8.13 (q, J = 5.2 Hz, 3H), 7.86–7.79 (m, 2H), 7.74 (m, 1H), 7.21 (d, J = 8.6 Hz, 1H), 7.07 (d, J = 8.0 Hz, 2H), 7.02 (dd, J = 8.1, 2.0 Hz, 1H), 2.29 (s, 3H), 2.16 (s, 3H). ^{13}C NMR (100 MHz, DMSO-d_6) δ 177.8, 143.9, 140.6, 138.9, 136.5, 135.8, 135.8, 135.8, 135.4, 133.7, 131.9, 131.3, 131.1, 130.8, 130.8, 130.7, 130.3, 129.1, 128.7, 128.5, 127.0, 125.4, 124.0, 122.7, 21.0, 18.1.

(*E*)-4-{[2-((2,6-Dimethylphenyl)carbamothioyl)hydrazineylidene]methyl},-2-nitrophenyl naphthalene-2-sulfonate (6r)

Yellow solid, m.p. 239–241 °C, Yield 82 %. ^{1}H NMR (400 MHz, DMSO-d_6) δ 12.00 (s, 1H), 10.04 (s, 1H), 8.67 (d, J = 2.1 Hz, 1H), 8.61 (d, J = 2.0 Hz, 1H), 8.26 (dd, J = 8.5, 3.0 Hz, 2H), 8.16–8.10 (m, 3H), 7.86–7.80 (m, 2H), 7.74 (m, 1H), 7.21 (d, J = 8.6 Hz, 1H), 7.15–7.10 (m, 3H), 2.17 (s, 6H). ^{13}C NMR (100 MHz, DMSO-d_6) δ 177.5, 144.0, 140.6, 138.9, 137.3, 136.8, 135.8, 135.4, 133.8, 131.9, 131.3, 130.8, 130.8, 130.7, 130.3, 128.7, 128.5, 128.1, 127.5, 125.4, 123.9, 122.7, 18.4.

(*E*)-4-{[2-((2-Ethylphenyl)carbamothioyl)hydrazineylidene]methyl}-2-nitrophenyl naphthalene-2-sulfonate (6 s)

Yellow solid, m.p. 230–232 °C, Yield 83 %. ^{1}H NMR (400 MHz, DMSO-d_6) δ 12.02 (s, 1H), 10.14 (s, 1H), 8.65 (d, J = 2.1 Hz, 1H), 8.61 (d, J = 2.0 Hz, 1H), 8.28–8.23 (m, 2H), 8.14 (m, 3H), 7.87–7.80 (m, 2H), 7.74 (m, 1H), 7.32–7.18 (m, 5H), 2.57 (q, J = 7.6 Hz, 2H), 1.13 (t, J = 7.6 Hz, 3H). ^{13}C NMR (100 MHz, DMSO-d_6) δ 178.1, 143.9, 141.8, 140.6, 139.0, 137.9, 135.8, 135.4, 133.7, 131.9, 131.3, 130.8, 130.8, 130.7, 130.3, 129.8, 128.8, 128.7, 128.5, 127.7, 126.4, 125.4, 124.0, 122.7, 24.5, 14.6.

(*E*)-4-{[2-((3-Methoxyphenyl)carbamothioyl)hydrazineylidene]methyl}-2-nitrophenyl naphthalene-2-sulfonate (6 t)

Yellow solid, m.p. 188–190 °C, Yield 78 %. ^{1}H NMR (400 MHz, DMSO-d_6) δ 12.06 (s, 1H), 10.22 (s, 1H), 8.62 (d, J = 2.0 Hz, 2H), 8.26 (dd, J = 8.4, 5.0 Hz, 2H), 8.19 (dd, J = 8.7, 2.1 Hz, 1H), 8.15 (d, J = 8.1 Hz, 2H), 7.87–7.80 (m, 2H), 7.74 (m, 1H), 7.28 (t, J = 8.1 Hz, 1H), 7.23 (d, J = 8.6 Hz, 1H), 7.17 (t, J = 2.2 Hz, 1H), 7.11–7.07 (m, 1H), 6.81 (m, 1H), 3.76 (s, 3H). ^{13}C NMR (100 MHz, DMSO-d_6) δ 176.8, 159.5, 143.9, 140.7, 140.4, 139.5, 135.8, 135.2, 133.7, 131.9, 131.3, 130.9, 130.8, 130.7, 130.3, 129.3, 128.7, 128.5, 125.4, 124.4, 122.7, 118.9, 112.4,

111.6, 55.6.

3.5. Metal chelating assay

The metal-chelating ability was evaluated with slight modification based on the method described by Dinis et al. [56]. The Fe^{2+}-binding capacity was determined spectrophotometrically at 562 nm. Briefly, three different concentrations (9–76 nM) of the test compounds dissolved in methanol (0.4 mL) were added to a solution containing $FeCl_2$ (0.1 mL, 0.6 mM). The reaction was initiated by the addition of ferrozine solution (0.1 mL, 5 mM). The mixture was gently mixed and allowed to stand at room temperature for 10 min. Finally, the absorbance was measured at 562 nm using spectrophotometer [56].

3.6. Carbonic anhydrase activity assay

Sepharose-4B-L-Tyrosine-Sulfanilamide affinity column chromatography was used to purify the hCA isoenzymes. Sepharose-4B-L-Tyrosine-Sulfanilamide was employed in this method as a chromatographic assay matrix. In accordance with Verpoorte et al.'s [57]. description in a prior work, both CA isoenzyme activity was measured. The substrate that was employed was *p*-nitrophenylacetate (PNA). As explained in detail, the amount of protein was measured during the purification processes using the Bradford method. As in earlier studies [58–62] solution preparations and activity measurement amounts were carried out. One μmol of *p*-nitrophenyl acetate hydrolyzed to p-nitrophenol and acetate in one minute is considered one enzyme unit of CA I and II esterase activities [63].

4. Conclusion

In conclusion, both *in vitro* and *in silico* studies of 4-formyl-2-nitrophenyl naphthalene-2-sulfonate-based thiosemicarbazones demonstrated their significant therapeutic potential as hCA I and hCA II inhibitors. The synthesized compounds demonstrated notable inhibitory activity, with IC_{50} values ranging from 88.43 ± 3.25 nM to 380.07 ± 8.32 nM for hCA I, and 88.43 ± 3.25 nM to 277.37 ± 3.91 nM for hCA II. Notably, **6 l** exhibited the most potent inhibition, showing IC_{50} values of 88.43 ± 3.25 nM for hCA I and 61.82 ± 0.60 nM for hCA II-surpassing the reference drug acetazolamide (IC_{50} = 290.50 ± 9.12 nM for hCA I and 177.03 ± 6.08 nM for hCA II). Molecular docking studies revealed strong binding interactions with key residues in the CA active site, while ADME predictions indicated favorable pharmacokinetic properties, further supporting their drug-likeness. These findings support further structural optimization and biological evaluation of these thiosemicarbazones as promising candidates for the development of more effective and selective CA inhibitors. Overall, this study serves as a valuable foundation for the design and development of novel enzyme inhibitors with potential relevance to future CA therapies. Among the most potent pro-oxidants in both food and pharmacological systems are Fe^{2+} ions, which readily form complexes with ferrozine. The formation of the ferrozine-Fe^{2+} complex is disrupted in the presence of Fe^{2+}-chelating agents, leading to a decrease in the characteristics red coloration of the complex. In this context, several of the synthesized compounds notably (**6 h, 6 l, 6n,** and **6f**) demonstrated potential as effective metal chelators and could be further explored for related applications.

CRediT authorship contribution statement

Khawar Abbas: Methodology, Investigation. **Muhammad Islam:** Software, Investigation. **Muhammad Tayyab:** Investigation. **Mariya al-Rashida:** Software, Investigation. **Parham Taslimi:** Investigation, Data curation. **Talha Islam:** Software, Investigation. **Nastaran Sadeghian:** Methodology, Investigation. **Halil Şenol:** Investigation, Conceptualization. **Abdullah K. Alanazi:** Investigation, Funding acquisition. **Silvia Schenone:** Writing – review & editing. **Zahid Shafiq:** Writing – original draft, Conceptualization.

Funding

This research was funded by Taif University, Saudi Arabia, project No (TU-DSPP-2024-16)

Declaration of competing interest

The authors declare that they have no known competing financial interests or personal relationships that could have appeared to influence the work reported in this paper.

Acknowledgement

The authors extend their appreciation to Taif University, Saudi Arabia, for supporting this work through project number (TU-DSPP-2024-16). Z. Shafiq is thankful to the ORIC, BZ University, Multan, Pakistan.

Appendix A. Supplementary data

Supplementary data to this article can be found online at https://doi.org/10.1016/j.bioorg.2025.109243.

Data availability

Data will be made available on request.

References

[1] A. Rasool, Z. Batool, M. Khan, S.A. Halim, Z. Shafiq, A. Temirak, M.A. Salem, T. E. Ali, A. Khan, A. Al-Harrasi, Sci. Rep. 12 (2022) 16095.
[2] M. Trawally, K. Demir-Yazıcı, A. Angeli, K. Kaya, A. Akdemir, C.T. Supuran, Ö. Güzel-Akdemir, Anti-cancer agents in medicinal chemistry-anti-cancer agents 24, 2024, pp. 649–667.
[3] N. Lemon, E. Canepa, M.A. Ilies, S. Fossati, Front. Aging Neurosci. 13 (2021) 772278.
[4] H. Şenol, G. Çelik Turgut, A. Şen, R. Sağlamtaş, S. Tuncay, İ. Gülçin, G. Topçu, Med. Chem. Res. 32 (2023) 694–704.
[5] A. Aspatwar, N.K. Parvathaneni, H. Barker, E. Anduran, C.T. Supuran, L. Dubois, P. Lambin, S. Parkkila, J.Y. Winum, J. Enzyme Inhib. Med. Chem. 35 (2020) 109–117.
[6] L. Ciccone, C. Cerri, S. Nencetti, E. Orlandini, Molecules 26 (2021).
[7] C.B. Mishra, S. Kumari, A. Angeli, S. Bua, M. Buonanno, S.M. Monti, M. Tiwari, C. T. Supuran, Eur. J. Med. Chem. 156 (2018) 430–443.
[8] A. Aspatwar, M.E. Tolvanen, H. Barker, L. Syrjänen, S. Valanne, S. Purmonen, A. Waheed, W.S. Sly, S. Parkkila, Physiol. Rev. 102 (2022) 1327–1383.
[9] I.S. Ismail, Curr. Diabetes Rev. 14 (2018) 108–112.
[10] A. Er, Lett. Drug Des. Discovery 20 (2023) 1427–1436.
[11] N. Le Roy, D.J. Jackson, B. Marie, P. Ramos-Silva, F. Marin, Front. Zool. 11 (2014) 1–16.
[12] M. Tasleem, S. Ullah, A. Khan, S.N. Mali, S. Kumar, B. Mathew, A. Oneto, F. Noreen, G.E. Eldesoky, S. Schenone, A. Al-Harrasi, Z. Shafiq, RSC Adv 14 (2024) 21355–21374.
[13] F.P. Busardò, A.F. Lo Faro, A. Sirignano, R. Giorgetti, J. Carlier, Arch. Toxicol. 96 (2022) 1989–2001.
[14] S. Ghorai, S. Pulya, K. Ghosh, P. Panda, B. Ghosh, S. Gayen, Bioorg. Chem. 95 (2020) 103557.
[15] S. Zareei, M. Mohammadi-Khanaposhtani, M. Adib, M. Mahdavi, P. Taslimi, J. Mol. Struct. 1271 (2023) 134114.
[16] S. Giovannuzzi, C.T. Supuran, Trends Pharmacol. Sci. 46 (2025) 836–847.
[17] S. Kumar, S. Rulhania, S. Jaswal, V. Monga, Eur. J. Med. Chem. 209 (2021) 112923.
[18] M. Bozdag, F. Carta, M. Ceruso, M. Ferraroni, P.C. McDonald, S. Dedhar, C. T. Supuran, J. Med. Chem. 61 (2018) 6328–6338.
[19] C.B. Mishra, M. Tiwari, C.T. Supuran, Med. Res. Rev. 40 (2020) 2485–2565.
[20] A. Di Fiore, C. Pedone, J. Antel, H. Waldeck, A. Witte, M. Wurl, A. Scozzafava, C. T. Supuran, G. De Simone, Bioorg. Med. Chem. Lett. 18 (2008) 2669–2674.
[21] A. Moradi, H. Adibi, V. Akbari, A.R. Jalalvand, Sensing Bio-Sensing Res. 37 (2022) 100516.
[22] F.S. Tokalı, P. Taslimi, B. Tüzün, A. Karakuş, N. Sadeghian, İ. Gülçin, J. Iran. Chem. Soc. 20 (2023) 2631–2642.
[23] F.S. Tokalı, P. Taslimi, M. Sadeghi, H. Şenol, ChemistrySelect 8 (2023) e202301158.
[24] F.S. Tokalı, Z. Alım, Ü. Yırtıcı, ChemistrySelect 8 (2023) e202204191.

[25] S.B. Zahra, A. Khan, N. Ahmed, M. Rafique, L. Fatima, I. Khan, J. Hussain, S. Khalid, H.A. Ogaly, M.M. Ahmed, Z. Shafiq, J. Mol. Struct. 1322 (2025) 140511.
[26] M. Islam, A. Khan, M.T. Shehzad, A. Hameed, N. Ahmed, S.A. Halim, M. Khiat, M. U. Anwar, J. Hussain, R. Csuk, Z. Shafiq, A. Al-Harrasi, Bioorg. Chem. 87 (2019) 155–162.
[27] G. Korkmaz, J. New Res. Sci. 13 (2024) 61–83.
[28] P. Singh, T. Narsinghani, Lett. Drug Design & Discovery 22 (5) (2025) 100059.
[29] H. Aftab, S. Ullah, A. Khan, M. Al-Rashida, T. Islam, K.A. Dahlous, S. Mohammad, H. Kashtoh, A. Al-Harrasi, Z. Shafiq, Sci. Rep. 14 (2024) 22645.
[30] Z. Batool, S.M. Dutt, M. Al-Rashida, N.E. Gelsleichter, J. Pelletier, J. Sévigny, T. Islam, H. Aftab, T.M. Almutairi, F. Çakır, Z. Shafiq, Bioorg. Chem. 163 (2025) 108717.
[31] F.S. Tokalı, H. Şenol, T.G. Katmerlikaya, A. Dağ, K. Şendil, J. Heterocyclic Chem. 60 (2023) 645–656.
[32] I. Munir, H. Aftab, A.A. Farooq, H. Şenol, P. Taslimi, N. Sadeghian, R.D. Alharthy, A. Rasool, U. Ghaffar, S. Schenone, Z. Shafiq, Bioorg. Med. Chem. 129 (2025) 118301.
[33] J. Eshal, H.Z. Tariq, J. Li, H. Aftab, H. Şenol, P. Taslimi, N. Sadeghian, R. D. Alharthy, M.S. Akram, R. Talib, Z. Shafiq, Bioorg. Chem. 155 (2025) 108118.
[34] H. Aftab, M. Islam, H. Şenol, Z. Batool, Ş. Ateşoğlu, F. Çakır, F. Akbaş, P. Taslimi, A. K. Alanazi, F. Noreen, Z. Shafiq, Sci. Rep. 15 (2025) 33402.
[35] M. Khalid, R. Jawaria, M.U. Khan, A.A.C. Braga, Z. Shafiq, M. Imran, H.M.A. Zafar, A. Irfan, ACS Omega 6 (2021) 16058–16065.
[36] R. Jawaria, M. Hussain, H.B. Ahmad, M. Ashraf, S. Hussain, M.M. Naseer, M. Khalid, M.A. Hussain, M. Al-Rashida, M.N. Tahir, Z. Shafiq, Inorg. Chim. Acta 508 (2020) 119658.
[37] C. Shen, M. Yang, J. Xu, C. Chen, K. Zheng, J. Shen, P. Zhang, RSC Adv. 7 (2017) 49436–49439.
[38] A. Köse, L.P. Köse, H. Şenol, N. Ulusoy-Güzeldemirci, J. Mol. Struct. 1325 (2025) 140937.
[39] F.S. Tokali, Y. Demir, I.H. Demircioglu, C. Turkes, E. Kalay, K. Sendil, S. Beydemir, Drug Dev. Res. 83 (2022) 586–604.
[40] A. Kamalı, R. Çakmak, M. Boğa, J. Chin. Chem. Soc. 69 (2022) 731–743.
[41] E. Başaran, R. Çakmak, S. Akkoc, S. Kaya, J. Mol. Struct. 1265 (2022) 133427.
[42] R. Çakmak, Erzincan Univ. J. Sci. Technol. 15 (2020) 659–669.
[43] F.S. Tokalı, Y. Demir, P. Tokalı, Ş. Ateşoğlu, H. Şenol, J. Biochem. Mol. Toxicol. 39 (2025) e70412.
[44] F.S. Tokalı, Y. Demir, Ş. Ateşoğlu, P. Tokalı, H. Şenol, Arch Pharm (Weinheim) 358 (2025) e70033.
[45] W. Xie, Z. Liu, D. Fang, W. Wu, S. Ma, S. Tan, K. Zheng, J. Mol. Struct. 1185 (2019) 240–258.
[46] L. Kang, X.-H. Gao, H.-R. Liu, X. Men, H.-N. Wu, P.-W. Cui, E. Oldfield, J.-Y. Yan, Mol. Divers. 22 (2018) 893–906.
[47] Z. Yan, B. Yu, X. Lan, X. Cui, D. Zhao, L. Qiu, H. Wang, W. Wang, L. Chen, L. Jin, J. Mol. Struct. 1308 (2024) 138331.
[48] H. Yakan, H. Muğlu, C. Türkeş, Y. Demir, M. Erdoğan, M.S. Çavuş, Ş. Beydemir, J. Mol. Struct. 1280 (2023) 135077.
[49] B. Akış, R. Çakmak, M. Şentürk, Chem. Biodivers. 21 (2024) e202401849.
[50] I. D'Agostino, G.E. Mathew, P. Angelini, R. Venanzoni, G. Angeles Flores, A. Angeli, S. Carradori, B. Marinacci, L. Menghini, M.A. Abdelgawad, J. Enzyme Inhib. Med. Chem. 37 (2022) 986–993.
[51] S. Jalil, S. Ullah, S.-O. Zaraei, R.M. Sbenati, A.I. Shahin, B.O. AlKubaisi, J. Pelletier, J. Sévigny, T.H. Al-Tel, J. Iqbal, Med. Chem. Res. 32 (2023) 869–883.
[52] S. Hashmi, S. Khan, Z. Shafiq, P. Taslimi, M. Ishaq, N. Sadeghian, H.S. Karaman, N. Akhtar, M. Islam, A. Asari, Bioorg. Chem. 107 (2021) 104554.
[53] M. Guney, A.G. Aggul, A. Erturk, I. Gulcin, ChemistrySelect 8 (2023) e202303054.
[54] T.V. Koksharova, T.S. Skakuun, I.V. Stoyanova, Russ. J. Gen. Chem. 91 (2021) 1057–1062.
[55] A. Korkmaz, E. Bursal, Chem. Biodivers. 19 (2022) e202200140.
[56] T.C. Dinis, V.M. Maderia, L.M. Almeida, Arch. Biochem. Biophys. 315 (1994) 161–169.
[57] J.A. Verpoorte, S. Mehta, J.T. Edsall, J. Biol. Chem. 242 (1967) 4221–4229.
[58] P. Taslimi, C. Caglayan, V. Farzaliyev, O. Nabiyev, A. Sujayev, F. Turkan, R. Kaya, İ. Gulçin, J. Biochem. Mol. Toxicol. 32 (2018) e22042.
[59] S. Ökten, M. Ekiz, Ü.M. Koçyiğit, A. Tutar, İ. Çelik, M. Akkurt, F. Gökalp, P. Taslimi, İ. Gülçin, J. Mol. Struct. 1175 (2019) 906–915.
[60] F. Turkan, A. Cetin, P. Taslimi, İ. Gulçin, Arch Pharm (Weinheim) 351 (2018) e1800200.
[61] H. Gul, A. Demirtas, G. Ucar, I. Gülçin, Lett. Drug. Des. Discov. 14 (2016).
[62] H.U. Celebioglu, Y. Erden, F. Hamurcu, P. Taslimi, O.S. Şentürk, Ü. Özmen, B. Tuzun, İ. Gulçin, J. Biomol. Struct. Dyn. 39 (2021) 5539–5550.
[63] S. Bal, R. Sağlamtaş, Y. Gok, A. Aktaş, M. Karaman, I. Gülçin, Bioorg. Chem. 94 (2019) 103468.